Supplementary Materials for

Gut Microbiota from Twins Discordant for Obesity Modulate Metabolism in Mice

Vanessa K. Ridaura, Jeremiah J. Faith, Federico E. Rey, Jiye Cheng, Alexis E. Duncan, Andrew L. Kau, Nicholas W. Griffin, Vincent Lombard, Bernard Henrissat, James R. Bain, Michael J. Muehlbauer, Olga Ilkayeva, Clay F. Semenkovich, Katsuhiko Funai, David K. Hayashi, Barbara J. Lyle, Margaret C. Martini, Luke K. Ursell, Jose C. Clemente, William Van Treuren, William A. Walters, Rob Knight, Christopher B. Newgard, Andrew C. Heath, Jeffrey I. Gordon*

* Corresponding author. E-mail: jgordon@wustl.edu

Published 6 September 2013 in *Science* **341**, 1241214 (2013)
DOI: 10.1126/science.1241214

This PDF file includes:

Materials and Methods

Production of NHANES-based diets

The National Health and Nutrition Examination Survey (NHANES; years 2003-2008; http://www.cdc.gov/nchs/nhanes.htm) was used to identify subsets of the adult (20-65 years old) USA population who consumed quantities in the lower tertile for saturated fat and the upper tertile for fruits and vegetables (LoSF/HiFV diet) or the upper tertile for saturated fat and lower tertile for fruits and vegetables (HiSF/LoFV diet). We identified key food subgroups and characterized foods using a modified version of the USDA's hierarchical food categories, which included 63 food subgroups within eight major food groups. For each food group providing 2-5% of total energy intake, we included only the food subgroup with the greatest average energy contribution. For food groups providing more than 5% of total energy intake, we included all food subgroups contributing at least 10% of that food group's energy and consumed by at least 10% of the NHANES subpopulation, in addition to those subgroups consumed by at least 20% of this subpopulation. One food item was selected to represent each food subgroup based on the food consumed by the greatest weighted percentage of people in the NHANES subpopulation. These selected foods were prepared, in relative quantities to represent the weight of the food subgroup, according to standard recipes then combined, homogenized, freeze-dried at -20°C by Van Drunen Farms (Momence, IL) and pelleted (Research Diets, Inc., New Brunswick, NJ). Pellets, stored in vacuumed-sealed plastic bags, were sterilized by gamma-irradiation (Steris Co, Libertyville, IL). The ingredients used to generate these two diets and the results of nutrient composition analysis are presented in **table S13**.

Animal husbandry

All experiments involving mice were performed using protocols approved by the Washington University Animal Studies Committee. Germ-free adult male C57BL/6J mice were maintained in plastic flexible film gnotobiotic isolators under a strict 12 h light cycle and fed an autoclaved low-fat, polysaccharide-rich chow (LF/HPP) diet (B&K Universal, East Yorkshire, U.K; diet 7378000) or the NHANES-based diets *ad libitum*.

For co-housing experiments, mice were gavaged with a given culture collection and singly-housed in a cage in an isolator dedicated to animals receiving the same collection. Five days after gavage, mice with the lean culture collection were introduced into cages containing mice harboring the obese co-twin's culture collection. Controls consisted of dually-housed Ln-Ln or Ob-Ob mice. Prior to co-housing, Aspen hardwood lab bedding (NEPCO) was replaced with freshly autoclaved material. Transplant recipients were maintained in separate cages within a gnotobiotic isolator dedicated to animals colonized with the same human donor microbiota, except in the case of co-housing experiments.

Collection of fecal samples from twin pairs discordant for obesity and transplantation of their uncultured fecal microbiota into germ-free mice

Adult female twin pairs with a BMI discordance ranging from 5.5-10 kg/m^2 were recruited for this study. Procedures for obtaining their consent to provide fecal samples

were approved by the Washington University Human Studies Committee. A single fecal sample was collected at t=0 and another 2 months later from each subject. Information about body-weight was updated at the time of each fecal sample collection. Each sample was frozen immediately at -20^{o}C, shipped in a frozen state to a biospecimen repository overseen by one of the authors (A.C.H), and then de-identified. All samples were subsequently stored at -80°C until the time of processing.

A given human fecal sample (from the second time point) was homogenized with a mortar and pestle while submerged in liquid nitrogen. A 500 mg aliquot of the pulverized frozen material was then diluted in 5 mL of reduced PBS (PBS supplemented with 0.1% Resazurin (w/v), 0.05% L-cysteine-HCl) in an anaerobic Coy chamber (atmosphere, 75% N_2, 20% CO_2, 5% H_2) and then vortexed at room temperature for 5 min. The suspension was allowed to settle by gravity for 5 min, after which time the clarified supernatant was transferred to an anaerobic crimped tube that was then transported to the gnotobiotic mouse facility. The outer surface of the tube was sterilized by exposure for 20 min to chlorine dioxide in the transfer sleeve attached to the gnotobiotic isolator, and then transferred into the isolator. A 1 mL syringe was used to recover a 200 μL aliquot of the suspension, which was subsequently introduced by gavage with a flexible plastic tube into the stomachs of each adult C57BL/6J germ-free recipient. Human microbiota transplant recipients were maintained in separate cages within an isolator dedicated to mice colonized with the same donor microbiota, except in the case of co-housing experiments.

Quantitative magnetic resonance (qMR) analysis of body composition
Body composition was defined using an EchoMRI-3in1 instrument (EchoMRI, Houston, TX). Mice were transported from their gnotobiotic isolators to the MR instrument in a HEPA filter-capped glass vessel. Fat mass, lean body mass and tissue-free body water were measured as indicated in the text for each experimental paradigm.

Sample collection from gnotobiotic mice
Fecal samples were collected at defined times after gavage from the mouse. At the time of sacrifice, lumenal contents were collected as previously described (*50*) at defined positions along the length of the gut (stomach, small intestinal segments 1,2,5,9,13 and 15 after its division into 16 equal-sized segments, cecum, and proximal and distal halves of the colon). Both epididymal fat pads as well as liver were recovered from each animal by dissection, weighed and flash frozen for transcriptional analysis.

Immune profiling
Spleens and MLNs were recovered by dissection from each mouse colonized with an intact fecal microbiota from a lean or obese co-twin. Each tissue sample was forced through 70 μm or 100 μm-diameter cell strainers (while bathed in PBS/0.1% BSA) to create single cell suspensions (*51*). Colonic and small intestinal lamina propria cells were prepared based on a previously described procedure (*52*). Cells from each of these sources were then plated in a 96-well, round bottom plastic plate, and incubated with anti-CD16/CD32 Fc block (eBiosciences) for 20 min at 4^{o}C to prevent non-specific staining in subsequent steps. Cells were washed in 200 μL of PBS/0.1%BSA, centrifuged

at 450 x g for 5 min and then surface stained with appropriate cocktails of anti-CD4 (labeled with APC or PerCp; BD Biosciences), TCR-β (labeled with FITC or PerCp; BD), CD44 (labeled with PE; BD Biosciences), CD62L (PE-Cy7; BD Biosciences) for 20 min at 4°C. Following staining, cells were washed twice as above, fixed overnight at 4°C using FoxP3 Fixation/Permeabilization buffer (Fix.Perm, eBioscience), washed twice to remove all buffer, and then incubated with Permeabilization Buffer (eBioscience) supplemented with normal rat serum (final concentration 2%) for 1h at 4°C. Cells were placed in a cocktail of anti-Ki-67 (FITC:BD) and anti-FoxP3 (eFluor 450; eBioscience) for 20 min at 4°C, washed twice in Permeabilization buffer and acquired on an LSI II flow cytometer (Becton Dickinson). Data were analyzed using FlowJo software (Treestar).

Multiplex pyrosequencing of amplicons generated from bacterial 16S rRNA genes
Genomic DNA was extracted from feces and gut contents using a bead-beating protocol (*2*). Briefly, a ~500 mg aliquot of each pulverized frozen human fecal sample, or mouse fecal pellets (~50 mg), or stomach, small intestinal, cecal or colonic contents (~20 mg each) were re-suspended in a solution containing 500µL of extraction buffer [200mM Tris (pH 8.0), 200mM NaCl, 20mM EDTA], 210µL of 20% SDS, 500µL of phenol:chloroform:isoamyl alcohol (pH 7.9, 25:24:1, Ambion) and 500µL of a slurry of 0.1-mm diameter zirconia/silica beads. Cells were then mechanically disrupted using a bead beater (BioSpec Products, Bartlesville, OK; maximum setting for 3 min at room temperature), followed by extraction with phenol:chloroform:isoamyl alcohol and precipitation with isopropanol.

Amplicons of ~330bp, spanning variable region 2 (V2) of the bacterial 16S rRNA gene, were generated by using modified primers 27F and 338R that incorporated sample-specific barcodes (*26*) and subjected to multiplex pyrosequencing (454 FLX Standard or Titanium chemistry as indicated in **table S1A**). V2-16S rRNA sequences generated using 454 FLX Titanium chemistry were trimmed to the length obtained using 454 FLX Standard chemistry (250-300 nt) and, together with the sequences generated using FLX Standard chemistry, were filtered for low quality reads and binned according to their sample-specific barcodes. Reads were clustered into 97%ID OTUs using UCLUST (*53*) and the Greengenes reference OTU database. Reads that failed to hit the reference dataset were clustered *de novo* using UCLUST. A representative OTU set was created using the most abundant OTU from each bin. Reads were aligned using PyNAST (*54*).

A training dataset for taxonomic assignments was created using a modified NCBI taxonomy from the 'Isolated named strains 16S' in the Greengenes database (*55*). This dataset was manually curated by (i) removing strains in 'Isolated named strains 16S' that had non-standard taxonomy or that were not members of the domain Bacteria, and (ii) grouping strain level taxonomy from Greengenes assignments under a single NCBI species assignment. This dataset is available at http://gordonlab.wustl.edu/SuppData.html and was used to train the Ribosomal Database Project (RDP) version 2.4 (*56*) classifier and to assign taxonomy to picked OTUs.

We validated this assignment strategy with a 'mock community' composed of evenly pooled DNA from 48 sequenced members of the human gut microbiota (**table S16**). We performed an initial simulation *in silico* by first trimming the 42 known 16S rRNA sequences to the length of variable region 2 (note that complete 16S rRNA sequences were not available in the draft assemblies of 4 of the 48 community members; see **table S16**). We could accurately assign 89% of species-level taxa compared with 15% correct taxonomic assignments blasting against Greengenes. Additionally, we could correctly assign 91% of genus-level taxa with RDP2.4 trained on the manually curated 'Isolated named strains 16S', versus 81% or 73% correct assignments with Greengenes and RDP2.2, respectively (**table S16**). Note that the lowest taxonomic assignment that is provided when using the RDP2.2 database that accompanies their scripts is at the genus-level.

DNA from this 48-member community was then used as a template to generate and sequence PCR amplicons from the V2 regions of their 16S rRNA genes; the resulting dataset was composed of 90,555 pyrosequencer reads from two technical replicates. We subsequently picked OTUs and assigned taxonomy to our sequenced mock community by (i) using the default strategy in QIIME (*57*) version 1.5 (where the RDP 2.2 classifier is trained on the Greengenes taxonomy at the genus level), (ii) Blasting against Greengenes, or (iii) employing the RDP 2.4 classifier trained on the manually curated Greengenes database of 'Isolated named strains 16S'. We found that we could accurately assign 90% of species-level taxa compared with 19% correct taxonomic assignments using Greengenes. Additionally, we could correctly assign 100% of the genus-level taxa with RDP2.4 trained on the manually curated 'Isolated named strains 16S' versus 93% or 90% assigned by Greengenes and RDP2.2, respectively, thereby demonstrating that this optimized taxonomy does better at assigning picked OTUs compared to either the RDP 2.2 classifier trained on the Greengenes' genus-level taxonomy or blasting against the Greengenes reference taxonomy (**table S17**).

Samples were rarefied to a depth of 800 OTUs/sample. The OTU table was filtered to preserve OTUs with a relative abundance $\geq 0.5\%$. This threshold was also used to define a species as invasive. The filtered table was then rarefied to a depth of 700 OTUs/sample; while not completely characterizing the microbiota of each individual this depth has sufficient power for the analyses presented in this work (*58*). Data analysis (beta-diversity calculations, PCoA clustering, Random Forests, microbial source tracking) was performed using QIIME v1.5 and Vegan R package version 1.17-4 (*59*).

When calculating invasion scores and fold-changes, we added a pseudo-count of 10% of the minimum relative abundance among all species-level taxa present in all samples to each species-level taxon in each sample analyzed.

Shotgun pyrosequencing of total community DNA

For multiplex shotgun pyrosequencing (454 FLX Titanium chemistry), each cecal DNA sample (n=45) was randomly fragmented by nebulization to 500-800 bp and subsequently labeled with one of 12 MIDs (Multiplex IDentifier; Roche) using the MID manufacturer's protocol (Rapid Library preparation for FLX Titanium). Equivalent

amounts of up to 12 MID-labeled samples were pooled prior to each pyrosequencer run. Shotgun reads were filtered to remove all reads <60 nt, LR70 reads with at least one degenerate base (N), or reads with two continuous and/or three total degenerate bases, plus all duplicates (defined as sequences whose initial 20 nt were identical and shared an overall identity of >97% throughout the length of the shortest read). In the case of human fecal DNAs, all sequences with significant similarity to human reference genomes (BLASTN with e-value $\leq 10^{-5}$, bitscore ≥ 50, percent identity $\geq 75\%$) were removed. Comparable filtering against the mouse genome was performed for reads produced from samples obtained from recipient gnotobiotic animals.

All resulting filtered sequences were queried against the KEGG database (v58) using BLASTX. Sequences were annotated as the best hit in the database if (i) they had an E-value $< 10^{-5}$, (ii) the bit score was > 50, and (iii) the query and subject were at least 50% identical after being aligned. If two entries were assigned as the best BLAST hit, the read was annotated with both entries (*34*). EC, and KEGG Pathway assignments were made using the "KO" file provided by KEGG version 58. A matrix containing the counts for each KEGG annotation for each sample was generated for analysis with ShotgunFunctionalizeR (*24*) (R package version 1.2-8).

Microbial RNA-Seq

Procedures for microbial RNA-Seq are described in our previous publications (*60-62*). In brief, each fecal pellet (~ 50mg), collected at 15 days post colonization (dpc) or 17 dpc, was suspended while frozen in 1mL of RNAprotect bacteria reagent (Qiagen), vortexed for 5 min at room temperature and centrifuged (10 min; 5,000 x g; 4°C). After decanting the supernatant, pelleted cells were suspended in 500µL of extraction buffer (200 mM NaCl, 20 mM EDTA), 210µL of 20% SDS, 500 µL of phenol:choloroform:isoamyl alcohol (pH 4.5, 125:24:1, Ambion), and 250 µL of acid-washed glass beads (Sigma-Aldrich, 212-300 µm diameter). Microbial cells were lysed by mechanical disruption using a bead beater (Biospec, maximum setting; 5 min at room temperature), followed by phenol:chloroform:isoamyl alcohol extraction and precipitation with isopropanol. RNA was treated with RNAse-free TURBO-DNAse (Ambion) and 5S rRNA and tRNAs were removed (MEGAClear columns, Ambion). A second DNAse treatment was performed (Baseline-ZERO DNAse; Epicenter). rRNA was initially depleted using MICROBexpress kit (Ambion) followed by a second MEGAClear purification. In addition, custom biotinylated oligonucleotides, directed against conserved regions of sequenced human gut bacterial rRNA genes were employed for streptavidin bead-based pulldowns. cDNA was synthesized using SuperScript II (Invitrogen), followed by second strand synthesis with RNAseH, *E. coli* DNA polymerase (NEB) and *E. coli* DNA ligase (NEB). Samples were sheared using a BioRuptor XL sonicator (Diagenode); 150-200 bp fragments were gel selected and prepared for sequencing.

Multiplex microbial cDNA sequencing was performed using an Illumina Hi-Seq2000 instrument to generate 23.7 ± 16.4 million unidirectional 101 nt reads per sample. Methods for microbial mRNA analysis are described in detail elsewhere (*61*). In brief, reads were split according to 4-bp barcodes used to label each of four samples pooled together per HiSeq lane. After dividing sequences by barcode, reads were mapped to

genes in a custom database of 148 sequenced human gut bacterial genomes using the Bowtie 2 algorithm (*63*). A minimum score threshold of 42 was selected based on the distribution of scores for the reads. If a read mapped to more than one location in a genome or to multiple genomes, the counts for each gene were added according to the gene's fraction of unique-match counts. Pseudocounts were added (i.e. 1 count) to each gene prior to normalization to account for different sampling depths (data expressed as reads/kb/million mapped reads).

Intra-peritoneal glucose tolerance test (IPGTT)

Glucose tolerance tests were performed by intra-peritoneal injection of 1 g D-glucose/kg body weight after a 4 hour fast in Ln-Ln or Ob-Ob animals colonized for 15 d with the culture collection from twin pair 1 and fed a LoSF/HiFV diet.

Insulin signaling

For insulin signaling experiments, 1U of insulin/kg body weight was administered, via the portal vein 3h after glucose administration for IPGTT, to Ln-Ln or Ob-Ob animals that had been colonized for 15 d with the Ob or Ln culture collections from DZ twin pair 1 and fed the LoSF/HiFV diet. Three minutes after injection, animals were sacrificed. Liver and soleus muscles were harvested and snap frozen in liquid nitrogen for analysis of insulin-mediated Akt phosphorylation by immunoblotting [pAkt-Thr308 and pAS160-Thr642; (*64*)].

Mass spectrometry analysis

Protocols for targeted and nontargeted MS-MS, GC-MS of cecal and fecal contents plus serum, and methods for data analysis are provided in our earlier publications (*61*).

Culturing fecal microbiota

Each human fecal sample was pulverized in liquid nitrogen and resuspended in pre-reduced PBS (0.1% Resazurin, 0.05% Cysteine/HCl; 15mL/g feces). Samples were subsequently vortexed for 5 min and allowed to settle by gravity for 5 min to permit large, insoluble particles to settle. The supernatant was diluted 1000-fold in pre-reduced PBS and plated on 150 mm diameter plates containing pre-reduced Gut Microbiota Medium [GMM; (*65*)]. Plates were incubated in a Coy chamber, under anaerobic conditions, for 7d at 37^{o}C. Colonies were subsequently harvested *en masse* from six plates by scraping (10 mL of pre-reduced PBS/plate). Glycerol (30%)/PBS stocks were stored in anaerobic glass vials at -80°C. A 200µL aliquot of the non-arrayed culture collection was introduced by gavage into each recipient germ-free mouse.

Subsampling the culture collection

Methods for creating clonally arrayed culture collections from frozen fecal samples were initially described in an earlier publication (*65*). We subsequently created a set of interfaces for a Precision XS robot (BioTek) so that picking, arraying, and archiving of fecal bacterial culture collections could be done with speed and economy within an anaerobic Coy chamber. Taxonomies were assigned to each strain in an arrayed collection by 454 Titanium V2-16S rRNA pyrosequencing, as previously described. Most strains (defined as having a unique V2-16S rRNA sequence) were found in more than one

well across the arrayed library. Therefore, several replicate wells of each strain were picked robotically from the 384-well plate, and streaked onto 8-well TYG_S-agar plates. Plates were incubated under anaerobic conditions in a Coy chamber for 3 d at 37°C. A single colony from each agar well was picked, grown in TYG_S and archived as a TYG_S/15% glycerol stock at -80°C.

Microbial genome analysis

Genomic DNA was extracted from individual strains, first by bead-beating in phenol:chloroform, followed by purification through a Qiagen 96-well PCR purification plate. A barcoded Illumina sequencing library was then prepared for each sample (250 ng DNA/strain; gel size-selected at 350-500 bp). Barcoded DNAs were subjected to multiplex sequencing in a HiSeq2000 instrument (101 nt paired-end reads; ≥34-fold coverage of each genome; mean coverage, 118-fold) and assembled using Velvet and Velvet Optimizer, version 2.1.7 (Velvet Optimizer parameters were: -s 31 -e 31 --t 1; mean N50 contig length, 86kb; see **table S12A** for details). Genes, tRNAs, and rRNAs were annotated using Glimmer3.0 (*66*), tRNAScan 1.23 (*67*), and RNAmmer 1.2 respectively (*68*). CAZyme family assignments were made as described in ref (*69*) (**table S12B**).

Analysis of phylogenetic structure of fecal microbiota from co-housed Ob^{ch} and Ln^{ch} animals

For each mouse in a given cage in a given gnotobiotic isolator, we calculated the Net Relatedness Index [NRI; (*33*)] for all fecal samples collected after co-housing (days 5,6,7,10,11 and 15 post-colonization). We did so by comparing all 97% ID OTUs (excluding singletons) from each fecal sample with a master phylogenetic tree, built from every OTU sequenced in this study. In short, the mean phylogenetic distance (MPD) was calculated as the average of the pairwise phylogenetic distances among all pairs of taxa in each tested fecal community (observed MPD). An expected MPD value, using the master tree built for this study, was calculated by randomly drawing communities of the same species richness, and calculating their MPD across a 1000 random draws. We compared the observed MPD to the expected MPD value using the algorithm employed in Phylocom4.1, and implemented by QIIME version 1.5. NRI is positive for communities that are clustered in a non-random pattern, and negative for non-random, over-dispersed communities. Significance was determined by one-sample *t*-test.

Shared 97% ID OTUs and shared branch length were calculated by identifying the OTUs for each mouse sampled at a given day in a given cage, and then calculating the (i) intersection of the OTUs between each mouse and their cagemate (for shared OTUs), and (ii) the total descending branch length of the intersection of the OTUs between cagemates (for shared branch length).

qRT-PCR

Epididymal fat pads were collected at the time of sacrifice and RNA was extracted using Trizol® (Invitrogen). Approximately 5ug of total RNA was used to prepare cDNA (superscript II, Invitrogen) and SYBR green qPCR thereafter. All data were normalized

to TBP endogenous controls and quantitative measures were obtained using the $\Delta\Delta C_T$ approach. The primer pairs used for *Prdm16*, *ElovL3*, *Ucp1*, *Pgc-1alpha*, *Cidea* and TBP were previously described in (*70, 71*).

Distal small intestine and liver were collected at the time of sacrifice and RNA was extracted using an initial Trizol® extraction, followed by a QIAGEN RNeasy Mini Kit purification (cat no. 74104, QIAGEN). Approximately 2mg of total RNA was used to prepare 20 µL of cDNA using the Invitrogen High capacity cDNA reverse transcription Kit (Life Technologies). cDNA was diluted 4X and 1mL of cDNA was used to run Taq-Man qPCR reactions, using TaqMan® Universal Master Mix II, without UNG, plus commercially available TaqMan primers to Fxr/Nr1h4 (Mm00436425_m1), Fgf15 (Mm01275900_g1) and Cyp7a1 (Mm00484150_m1). All data were normalized to the endogenous controls L32 ribosomal protein (RPL32; Mm02528467_g1) (Life Technologies).

Supplementary Results

Wave 5 assessment of adult female twin pairs in the MOAFTS study cohort

For the present study, to identify informative twin pairs, we surveyed data collected at the 5th wave of assessment from 1,539 female twin pairs who were 21-32 years old. There were 3,427 participants with height and weight data available for 3,416 (99.7%). 54.3% of the twin pairs were MZ as determined by zygosity questionnaire. The majority of participants (55.8%) were classified as lean (BMI 18.50-24.99 kg/m^2), while 21.9% were classified as overweight (25-29.99 kg/m^2), 18.3% as obese (≥30 kg/m^2), and 3.98% as underweight (<18.5 kg/m^2). African-Americans, who comprised 14.4% of the wave 5 sample, had significantly higher rates of overweight and obesity compared to European-Americans (32.5% and 36.6% vs. 20.1% and 15.2%, respectively; $p \leq 0.001$).

The mean difference in BMI between co-twins was 3.53 kg/m^2 (SD 3.78 kg/m^2). The mean difference in BMI was greater in DZ compared to MZ twin pairs (4.65 ± 4.58 kg/m^2 versus 2.60 ± 2.57 kg/m^2; $p \leq 0.001$). We identified BMI discordant twin pairs using two different definitions. If one co-twin was classified as obese (BMI>30 kg/m^2) and the other lean (<25 kg/m^2), then 5.72% of twin pairs were defined as BMI discordant (mean difference = 11.42 ± 4.09 kg/m^2). The rate of discordance was substantially lower for MZ pairs compared to DZ pairs (2.3% versus 9.9%; $p \leq 0.001$). Alternatively, when BMI discordance was defined as ≥8 kg/m^2, regardless of BMI category of the leaner co-twin, 5.2% of MZ pairs and 18.3% of DZ pairs were classified as discordant ($p \leq 0.001$). Written informed consent was obtained from all research participants, using procedures approved by the Washington University Human Studies Committee.

Efficient and reproducible capture of the organismal and microbial gene content of human fecal samples in gnotobiotic mouse recipients

Comparisons of the 'input' human fecal microbiota, and the 'output' mouse fecal communities surveyed two weeks after transplantation revealed that 74.7 ± 5.6% (SD) of family-level bacterial taxa present in the human donor community were represented in the microbiota of gnotobiotic mouse recipients (n=3-12 animals analyzed/microbiota; **table S2A-C**). Clusters of V2-16S rRNA reads sharing ≥97% nucleotide sequence identity (97% ID) were defined as species-level operational taxonomic units (OTUs).

Principal Coordinates Analysis (PCoA) of unweighted UniFrac distances (*72, 73*) based on the 97%ID OTU datasets revealed that transplanted microbial communities stabilized in recipient mice within 3d, and remained different up to 35d post colonization (**Fig. 1B, fig. S1D**). UniFrac is a distance metric that compares communities based on their shared evolutionary history. The unweighted version of the metric, which uses presence/absence rather than abundance data, is most appropriate for these studies because transfer from the human donor to the mouse recipient is expected to cause shifts in the relative ratios of taxa. Importantly, the overall phylogenetic architecture of the transplanted communities evolved in a reproducible way between singly-housed recipient mice within a given experiment for a given co-twin's microbiota, and between replicate experiments (**Fig. 1B**). Pairwise unweighted UniFrac comparisons of fecal samples and of communities sampled along the length of the guts of all transplant recipients demonstrated that the highest level of similarity occurred among mice colonized with the same human donor microbiota. Moreover, their microbiota exhibited significantly greater similarity to their human donor's microbiota than to mice colonized with the microbiota of their sibling or unrelated donors ($p \leq 0.05$ based on Student's *t*-test with Monte Carlo simulations, 100 iterations; see **Fig. 1C; fig. S1A; table S2D**).

Shotgun pyrosequencing of cecal DNA samples prepared from mice colonized with each of the eight human fecal microbiota disclosed that transplant recipients not only efficiently captured the organismal features of their human donor's microbiota but also the functions encoded by the donor's microbiome [n=3-8 mice sampled 15 d after transplantation/microbiota; n=45 cecal samples; 99.7 ± 0.2% of donor microbiome-assigned enzyme commission numbers (ECs) captured in recipient mice, with a significant correlation observed between the proportional representation of reads with a given assignable EC in donor and recipient microbiomes ($p \leq 0.0001$ Spearman's correlation; Spearman's *rho* = 0.88-0.92; **fig. S2; table S1B**)**].**

Identifying bacterial taxa that differentiate mice harboring transplanted community from lean versus obese co-twins

We used supervised machine learning using a Random Forest classifier to identify bacterial taxa that differentiate gnotobiotic mice harboring gut communities transplanted from all lean versus all obese co-twins (*74*). Using class-level taxa, the estimated generalization error of the trained model was 6.4%, indicating that we could predict if a sample came from a mouse colonized with a lean or obese human donor microbiota with 93.6% accuracy. Eight class-level taxa were identified as producing a mean decrease in classification accuracy of ≥1% each when they were ignored [Erysipelotrichi, Clostridia, Negativicutes, and an unidentified class (from the phylum Firmicutes); Betaproteobacteria and Deltaproteobacteria (phylum Proteobacteria); Bacteroidia (Bacteroidetes), and Verrucomicrobiae (Verrucomicrobia)] with members of the Negativicutes, Erysipelotrichi, Clostridia, and Deltaproteobacteria being most discriminatory (see **table S3** for phylum-, class-, order-, family-, genus- and species-level taxa significantly different between mice colonized with a lean versus an obese intact, uncultured microbiota, plus relative abundance in the two groups and the *p* value for the comparison calculated by ANOVA).

Efficient and reliable transfer of culture collections to gnotobiotic animals

Fig. S6A-D illustrates how capture of cultured bacterial taxa and their encoded gene functions was both efficient and reproducible within and between groups of recipient gnotobiotic mice. Captured members of the obese or lean co-twin's culture collection represented 83 ± 3% (obese) and 86 ± 8% (lean) of the family-level taxa that were successfully transplanted into mouse recipients of the corresponding intact uncultured fecal samples, and 63 ± 3% (obese) and 51 ± 8% (lean) of the family-level taxa that were present in the original donor fecal sample (see **table S7A-C** for a summary overview and a list of phylum-, class-, order-, family-, genus-level taxa, plus 97%ID OTUs). Moreover, shotgun sequencing of the cecal microbiomes of transplant recipients confirmed efficient capture of functional features represented in transplanted intact (non-cultured) microbiomes and recapitulation of their proportional representation as judged by EC content (**fig. S6C-E**).

Net Related Index Analysis

NRI is a measure of the standardized effect size of the mean phylogenetic distance between all possible pairs of taxa in a community (*33, 75*). A significantly positive NRI indicates that a community is more phylogenetically clustered than expected by chance alone; a significantly negative NRI indicates that a community is more phylogenetically dispersed than expected by chance (*33*). NRI values of transplanted cultured communities in co-housed Ln-Ln controls differed significantly from zero ($p \leq 0.001$, one sample *t*-test), while Ob communities in co-housed Ob-Ob controls did not ($p = 0.07$) **(fig. S9E, fig. S12A).** Moreover, the average total descending branch length and the total number of 97% ID OTUs was significantly higher in Ln-Ln than in Ob-Ob controls, supporting the concept that the transplanted Ln microbiota was phylogenetically over-dispersed (**fig. S12B-C**; $p \leq 0.0001$; two-way ANOVA; Dunnett's multiple comparison test). NRI confirmed that 10 d after co-housing, the phylogenetic structure of the fecal microbiota from Ob^{ch} animals had changed significantly from Ob-Ob controls, transforming into a lean-like, overly dispersed configuration [**fig. S9E**; $p \leq 0.001$ (one sample *t*-test to test divergence from zero); $p \leq 0.001$ (paired *t*-test to test difference between Ob controls and Ln, Ln^{ch} and Ob^{ch} NRI values)] with significantly more shared 97%ID OTUs and branch length with their Ln^{ch} cagemates ($p \leq 0.0001$, paired *t*-test; **fig. S12E-F**). These observations are consistent with Ln communities having non-overlapping species (i.e. species absent in the Ob microbiota) that can invade and establish themselves in the guts of Ob^{ch} cagemates. The observation that the most invasive taxa from the Ln community are members of the Bacteroidetes agrees with some reports that increased representation of members of this phylum are associated with leanness, both in the context of weight loss due to diet changes and bariatric surgery (*2, 76*).

Adaptive thermogenesis analysis of epididymal fat pads

We used qRT-PCR to measure expression of *Prdm16*, *ElovL3*, *Ucp1*, *Pgc-1α* and *Cidea* in the epididymal fat pads of Ob-Ob, Ln-Ln, Ob^{ch} and Ln^{ch} animals fed either the NHANES LoSF/HiFV or LF/HPP diets. These genes are associated with brite cells (browning of white adipose tissue) and are downregulated in the setting of reduced adaptive thermogenesis. The higher fat LoSF/HiFV diet resulted in a significant change (reduction) in expression of two of these genes [*PGC-1 α* (39.36±12.34%), *Cidea*

(66.49±10.87%) ($p<0.001$, two-way ANOVA)] in all groups of mice (Ob-Ob, Ln-Ln, Ob^{ch}, and Ln^{ch}): i.e. there was no significant microbiota effect (two-way ANOVA; $p > 0.05$).

Fig. S1

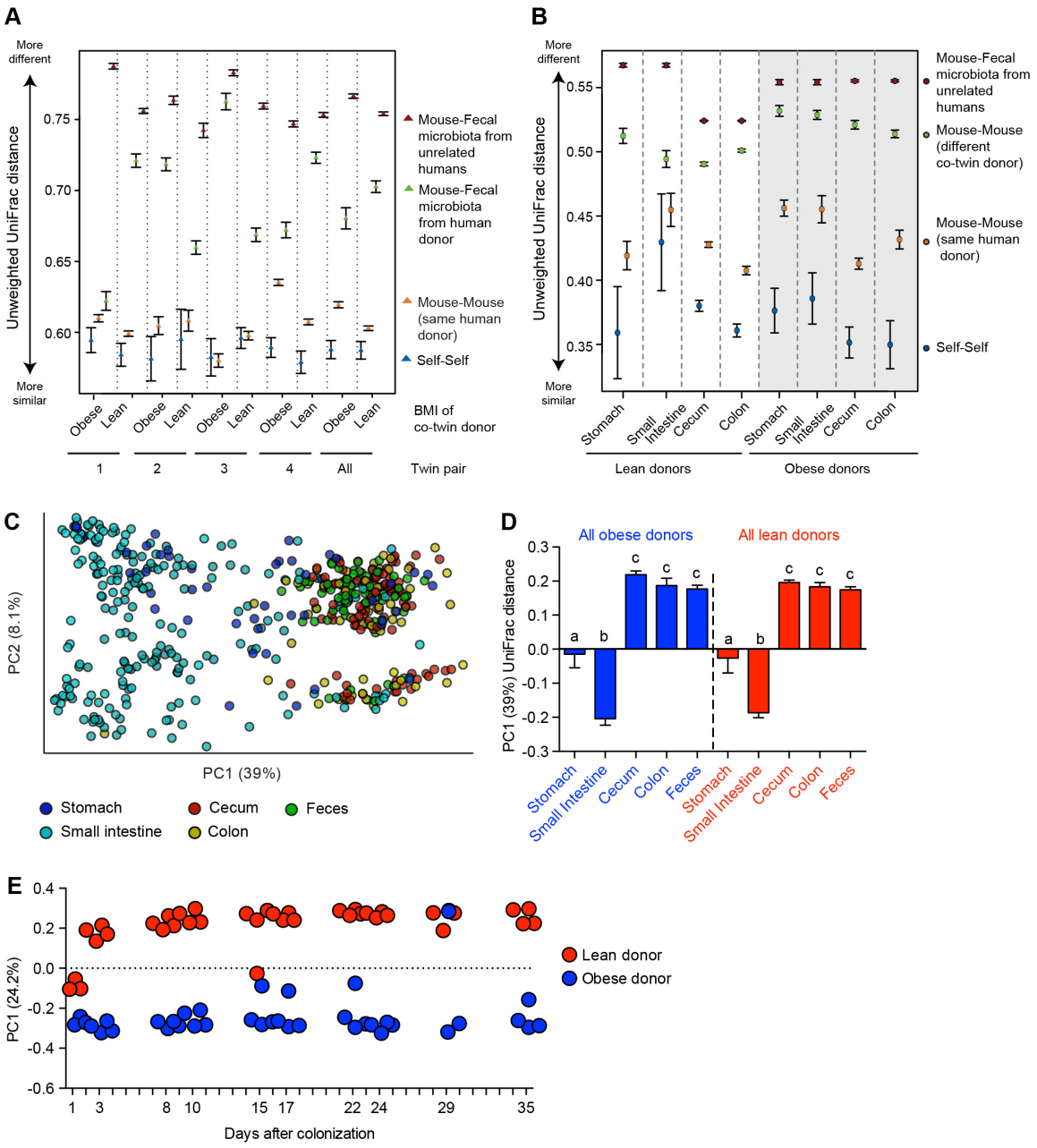

Transplantation of an intact uncultured fecal microbiota from an obese or a lean co-twin donor is reproducible within a group of recipient gnotobiotic mice. Data in A-D are from all four discordant twin pairs. **(A)** Transplantation of fecal microbiota from human donors to recipient mice captures interpersonal differences. Mean values ± SEM for pairwise unweighted UniFrac distance measurements are plotted. Abbreviations: 'Self-Self' comparison, same mouse sampled at different time points within a given experiment; 'Mouse-Mouse (same human donor)', mice colonized with the same human donor's fecal microbiota sample (3-8 mice/donor; 1-5 independent experiments/donor sample); 'Mouse-Fecal microbiota from human donor', comparison of fecal bacterial communities in a recipient group of mice versus their human donor's microbiota;

'Mouse-Fecal sample from unrelated humans', comparison of fecal microbiota from recipients of given donor's microbiota compared to the fecal microbiota of all other unrelated individuals (across twin pair comparison; this latter analysis involved two fecal samples obtained two months apart for each individual in each twin pair). See **table S2D** for results of statistical tests of observed differences in unweighted UniFrac distances. (**B)** Mean values ± SEM for pairwise UniFrac distance measurements are plotted. Abbreviations: 'Self-Self', comparison of community structures from different regions of the gut (note the small intestine was divided into 16 equal length segments with segment 1 being most proximal; segments 1,2,5,9,13, and 15 were analyzed separately and pairwise comparisons of segments performed to generate the mean value ± SEM that is plotted); 'Mouse-Mouse (same human donor)', mice colonized with the same human donor's fecal microbiota sample (3-8 mice/donor; 1-4 independent experiments/donor sample); 'Mouse-fecal microbiota from unrelated humans', comparison of fecal microbiota from gnotobiotic recipients of given donor's microbiota versus the fecal microbiota of all other unrelated humans (i.e. across twin pair comparison). *$p \leq 0.05$, ** $p \leq 0.001$; Student's *t*-test with Monte Carlo simulation, 100 iterations. **(C)** Principal coordinate analysis (PCoA), based on a weighted UniFrac distance metric, of samples collected along the length of the gut from mice humanized with a fecal sample obtained from lean or obese co-twins. **(D)** Comparison of communities along the length of the gut based on their positioning along principal component 1 of the ordination plot (PC1 explains 39% of the variation). The same letter indicates that the indicated intestinal segments exhibited no significant differences in the overall phylogenetic structures of their microbiota. Different letters are used to signify that the indicated intestinal segments have significant differences in their bacterial community structures (comparing segments with the same letter indicates that there were no significant differences in their bacterial community structures). Different letters indicate a *p*-value <0.05 based on results of one-way ANOVA with Holm- Šidák′s correction for multiple hypotheses. **(E)** PCoA of fecal samples collected from mice colonized with fecal microbiota of DZ twin pair 1 lean or obese co-twin and maintained on a LF/HPP mouse chow for 35 d. Community structure is maintained throughout the duration of the experiment.

Fig. S2

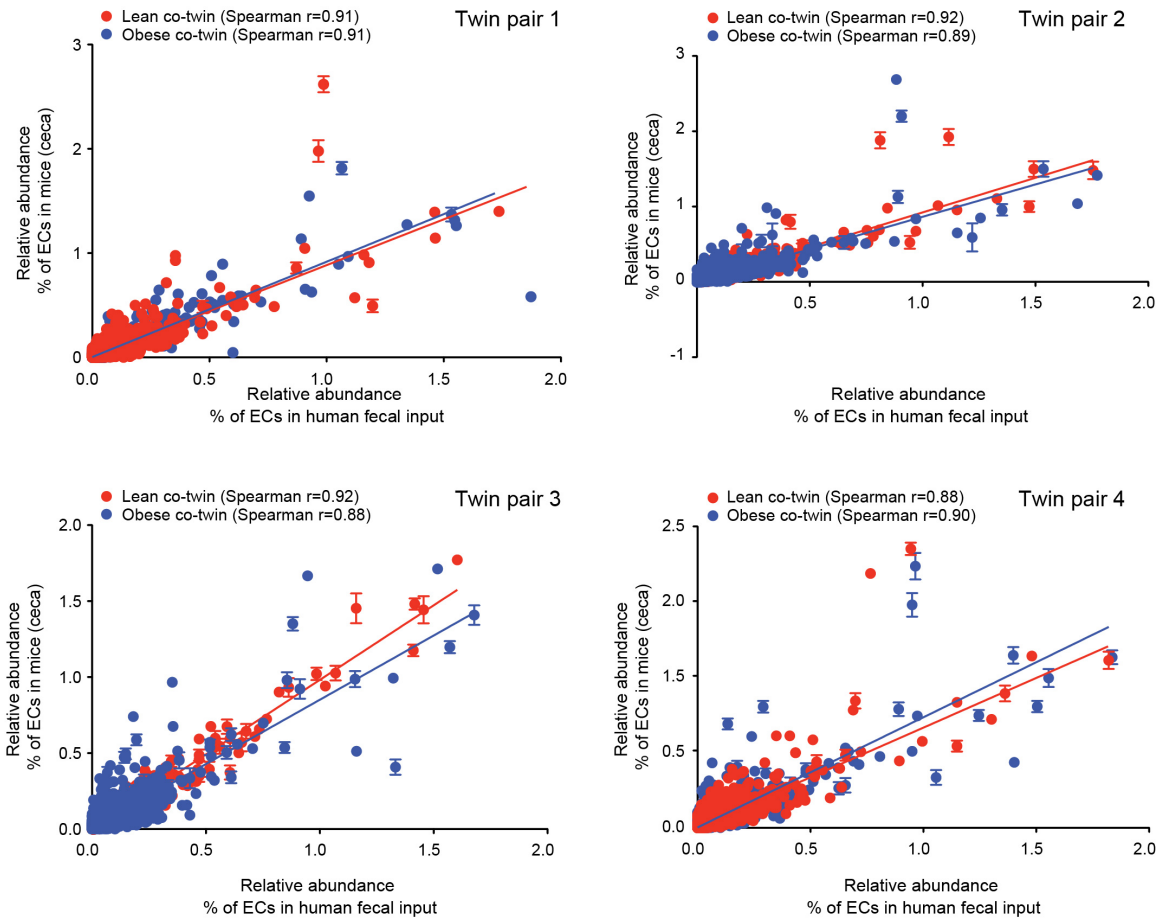

Correlation between the representation of genes with assigned KEGG EC annotations in each human donor's microbiome and their representation in the cecal microbiomes of the corresponding gnotobiotic mouse transplant recipients. Each circle represents an EC. Mean values ± SEM are plotted for each EC in a given group of mice (n=4 recipient mice/human donor). The Spearman correlation value (*rho*) is indicated and is significant in all cases ($p \leq 0.0001$).

Fig. S3

A

EC enriched in fecal transcriptome of mice colonized with a lean co-twin's microbiome

EC enriched in fecal transcriptome of mice colonized with an obese co-twin's microbiome

Metabolite enriched in the cecal metabolome of mice colonized with a lean co-twin microbiome

Metabolite enriched in the cecal metabolome of mice colonized with an obese co-twin microbiome

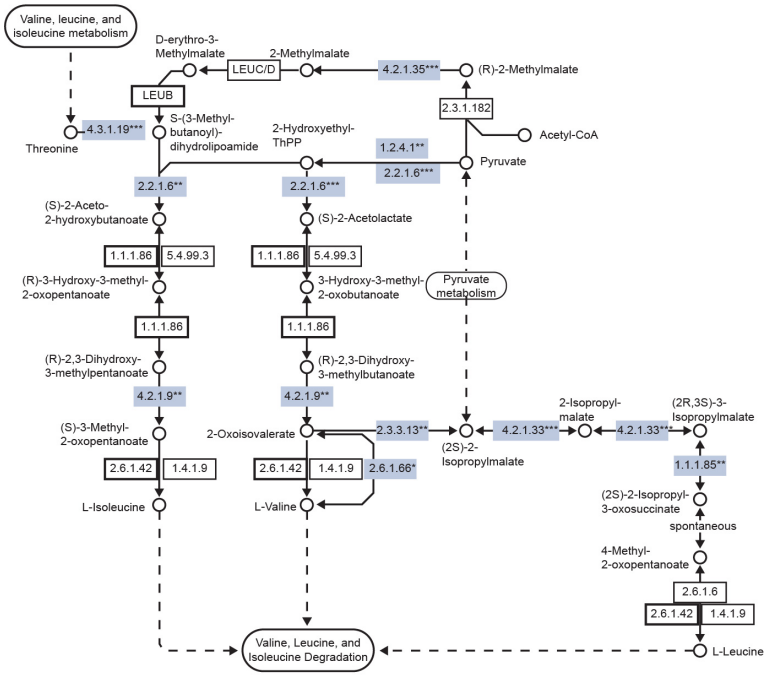

Valine, Leucine, and Isoleucine Biosynthesis

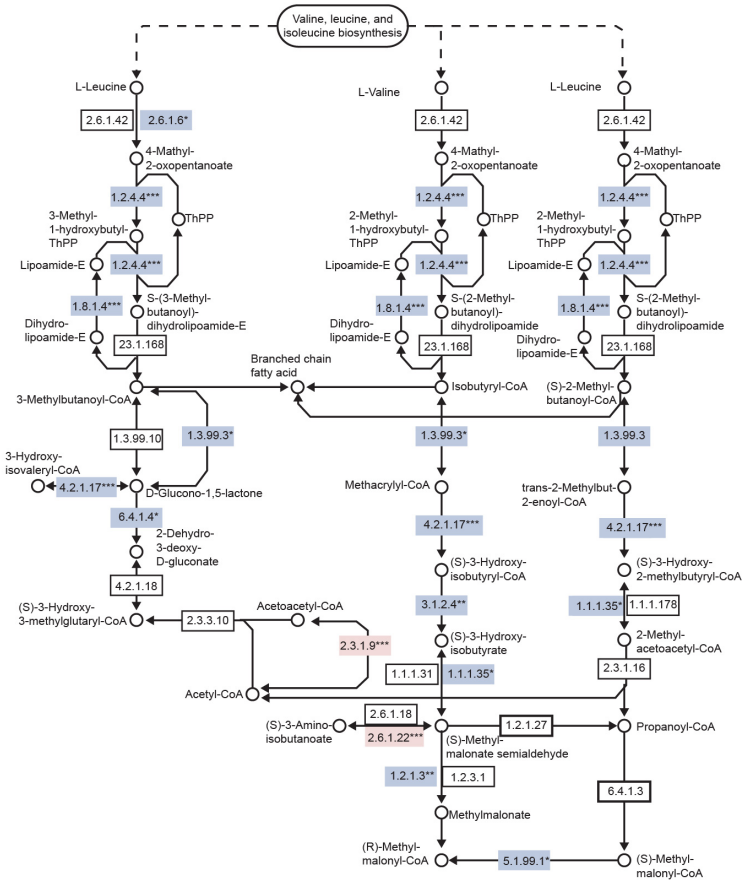

Valine, Leucine, and Isoleucine Degradation

B

Pentose Phosphate Pathway

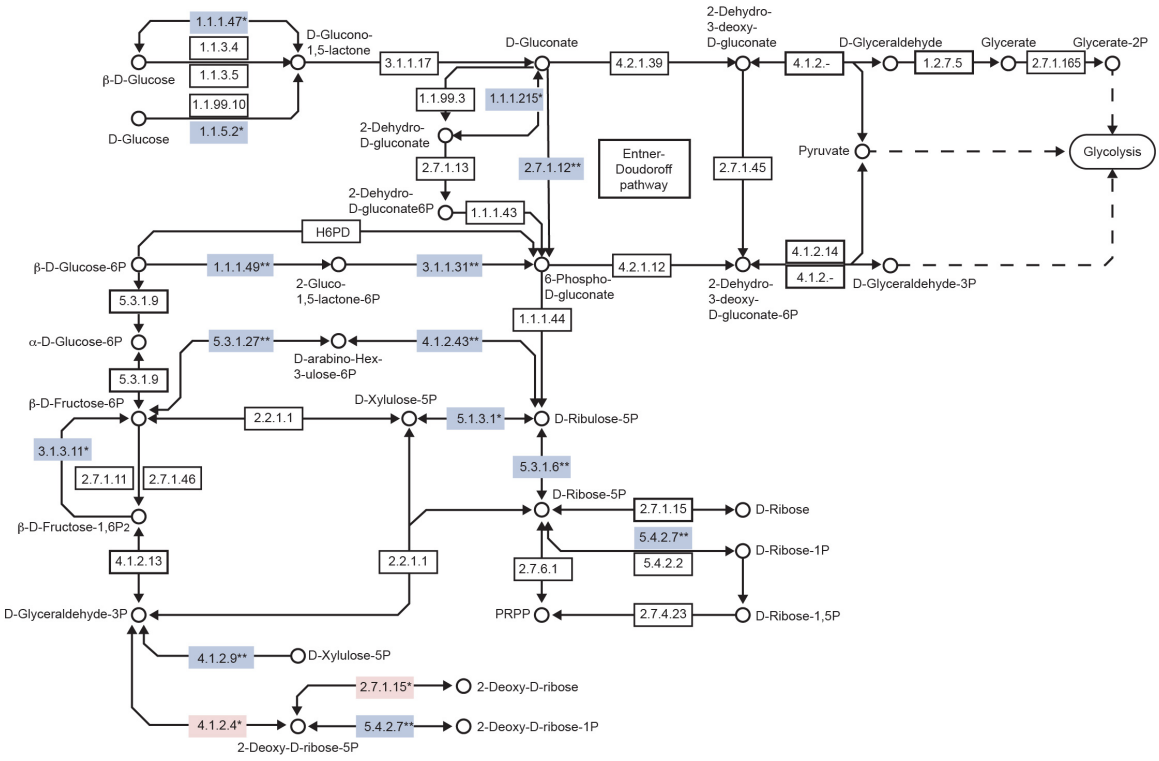

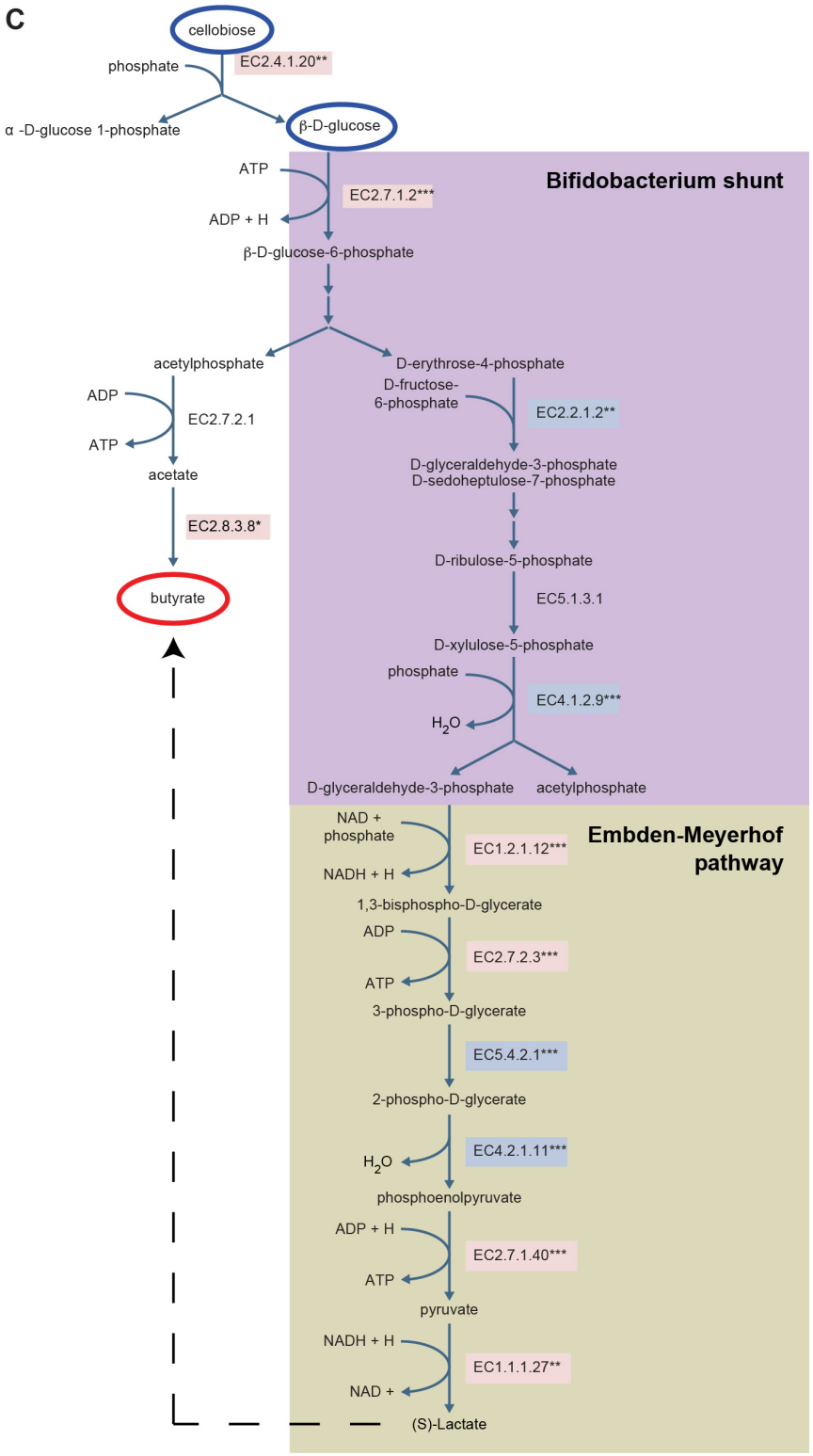
C
cellobiose
phosphate
EC2.4.1.20**
α -D-glucose 1-phosphate
β-D-glucose
Bifidobacterium shunt
ATP
EC2.7.1.2***
ADP + H
β-D-glucose-6-phosphate
acetylphosphate
ADP
EC2.7.2.1
ATP
acetate
EC2.8.3.8*
butyrate
D-erythrose-4-phosphate
D-fructose-
6-phosphate
EC2.2.1.2**
D-glyceraldehyde-3-phosphate
D-sedoheptulose-7-phosphate
D-ribulose-5-phosphate
EC5.1.3.1
D-xylulose-5-phosphate
phosphate
EC4.1.2.9***
H2O
D-glyceraldehyde-3-phosphate
acetylphosphate
Embden-Meyerhof
pathway
NAD +
phosphate
EC1.2.1.12***
NADH + H
1,3-bisphospho-D-glycerate
ADP
EC2.7.2.3***
ATP
3-phospho-D-glycerate
EC5.4.2.1***
2-phospho-D-glycerate
H2O
EC4.2.1.11***
phosphoenolpyruvate
ADP + H
EC2.7.1.40***
ATP
pyruvate
NADH + H
EC1.1.1.27**
NAD +
(S)-Lactate

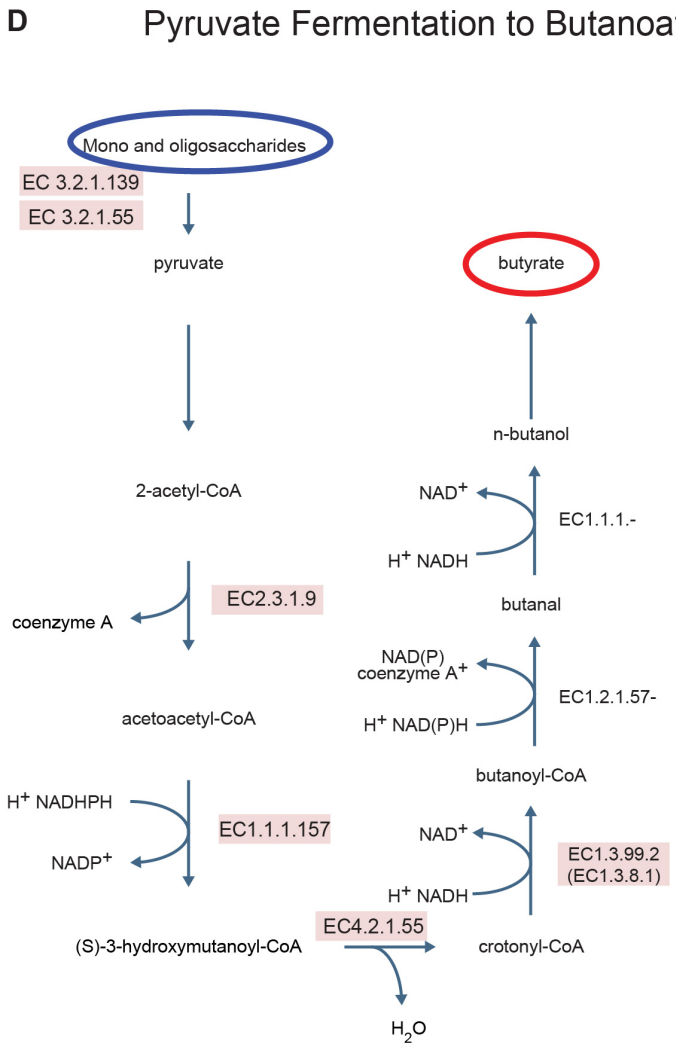

KEGG pathway maps of ECs whose representation was significantly different in the fecal meta-transcriptomes of mice with transplanted intact uncultured fecal microbial communities from obese versus lean co-twins. (A) KEGG 'Valine, Leucine, and Isoleucine Biosynthesis' and 'Degradation' pathway. **(B)** KEGG 'Pentose Phosphate Pathway'. **(C)** Overview of carbohydrate fermentation. **(D)** KEGG pathway 'Pyruvate Fermentation to Butyrate'. Blue indicates that the expressed EC or metabolites were significantly enriched in the fecal meta-transcriptomes of mice that received fecal microbiomes from obese twins compared to the fecal meta-transcriptomes of mice that had received fecal microbiomes from their lean co-twin siblings. Red indicates expressed ECs or metabolites that were significantly enriched in the fecal meta-transcriptomes of recipients of lean co-twin microbiomes. All ECs highlighted in Red or Blue were differentially expressed by transplanted microbiomes from at least two of the four discordant twin pairs. $*p \leq 0.0001$, $**p \leq 10^{-10}$, $***p \leq 10^{-30}$ (ShotgunFunctionalizeR; AIC value <5000). See **tables S4, S5** and **S6** for further details, including statistical analysis for each EC and KEGG Pathway (Shotgun FunctionalizerR and Random Forests) or metabolite (Student's *t*-test with Benjamini-Hochberg adjusted *p*-values).

Fig. S4

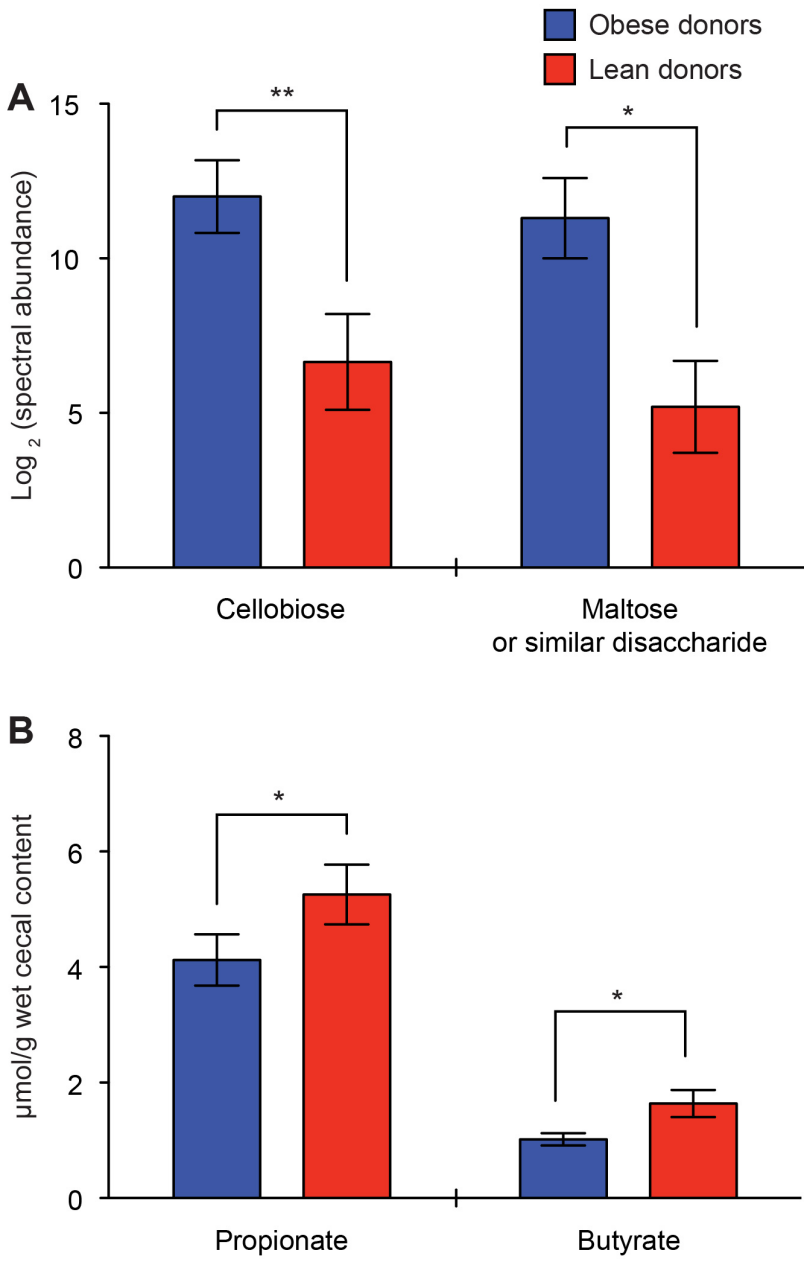

Metabolites with significant differences in their levels in the ceca of gnotobiotic recipients of obese compared to lean co-twin fecal microbiota transplants. (A) Cellobiose and 'maltose or a similar disaccharide' levels measured by nontargeted GC/MS. **(B)** Targeted GC/MS of cecal SCFA. *, $p \leq 0.05$; **, $p \leq 0.01$ (two-tailed unpaired Student's *t*-test).

Fig. S5

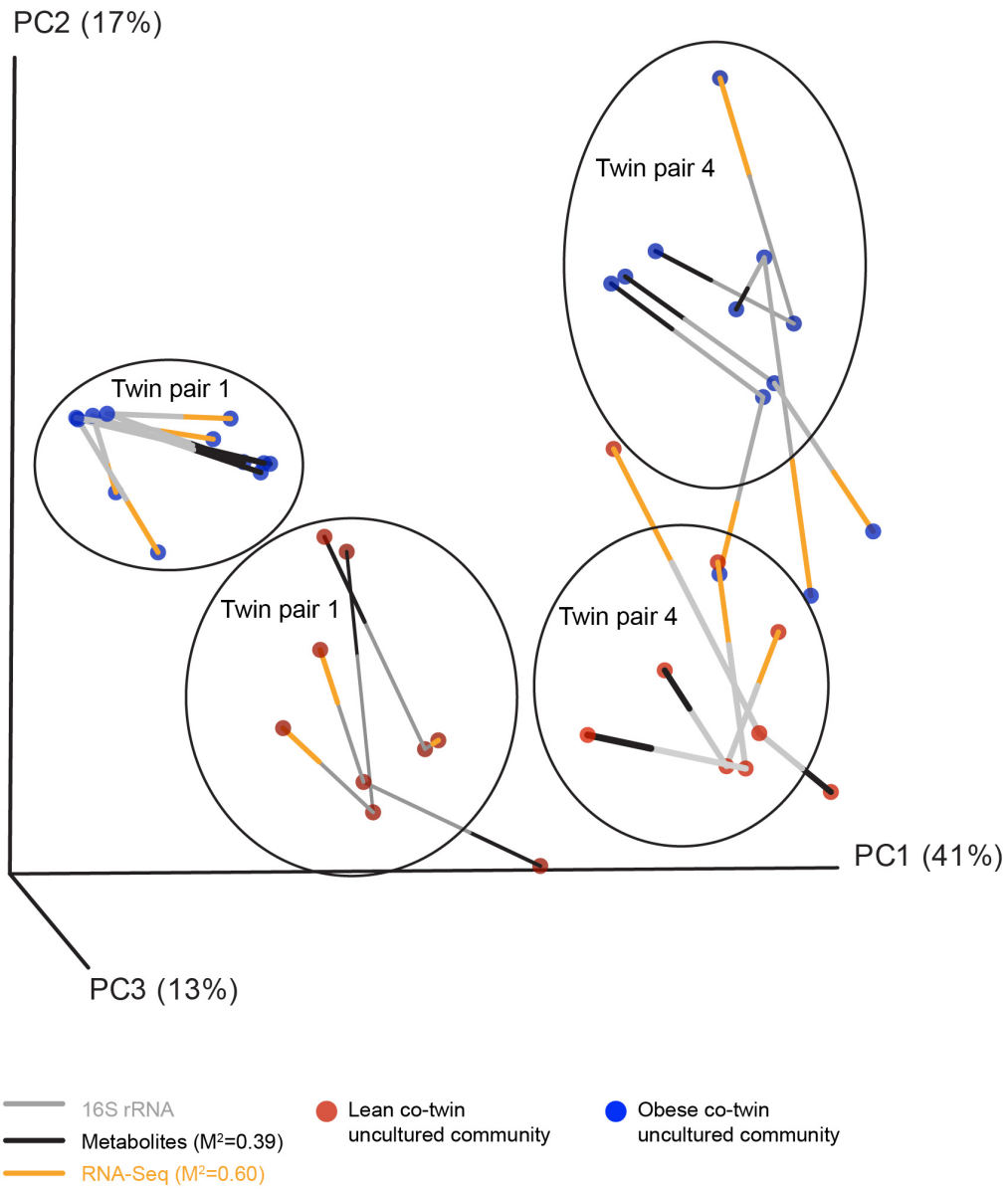

Comparison of bacterial 16S rRNA, microbial RNA-Seq and nontargeted GC/MS datasets from recipients of microbiome transplants from discordant DZ pair 1 and discordant MZ pair 4. Procrustes analysis based on Hellinger distance matrix and the following data-types: V2-16S rRNA (97%ID OTUs; communities denoted as circles linked to gray bars); nontargeted GC/MS (circle linked to black bars); and RNA-Seq (EC annotations assigned to transcripts in a given sample; circle linked to orange bars). A two-tailed pairwise Mantel test (with 100 iterations) between these three distance matrices confirmed that OTUs are highly correlated to the fecal transcriptome and fecal metabolome ($p \leq 0.01$). M^2 values for goodness of fit relative to the 16S rRNA datasets are shown.

Fig. S6

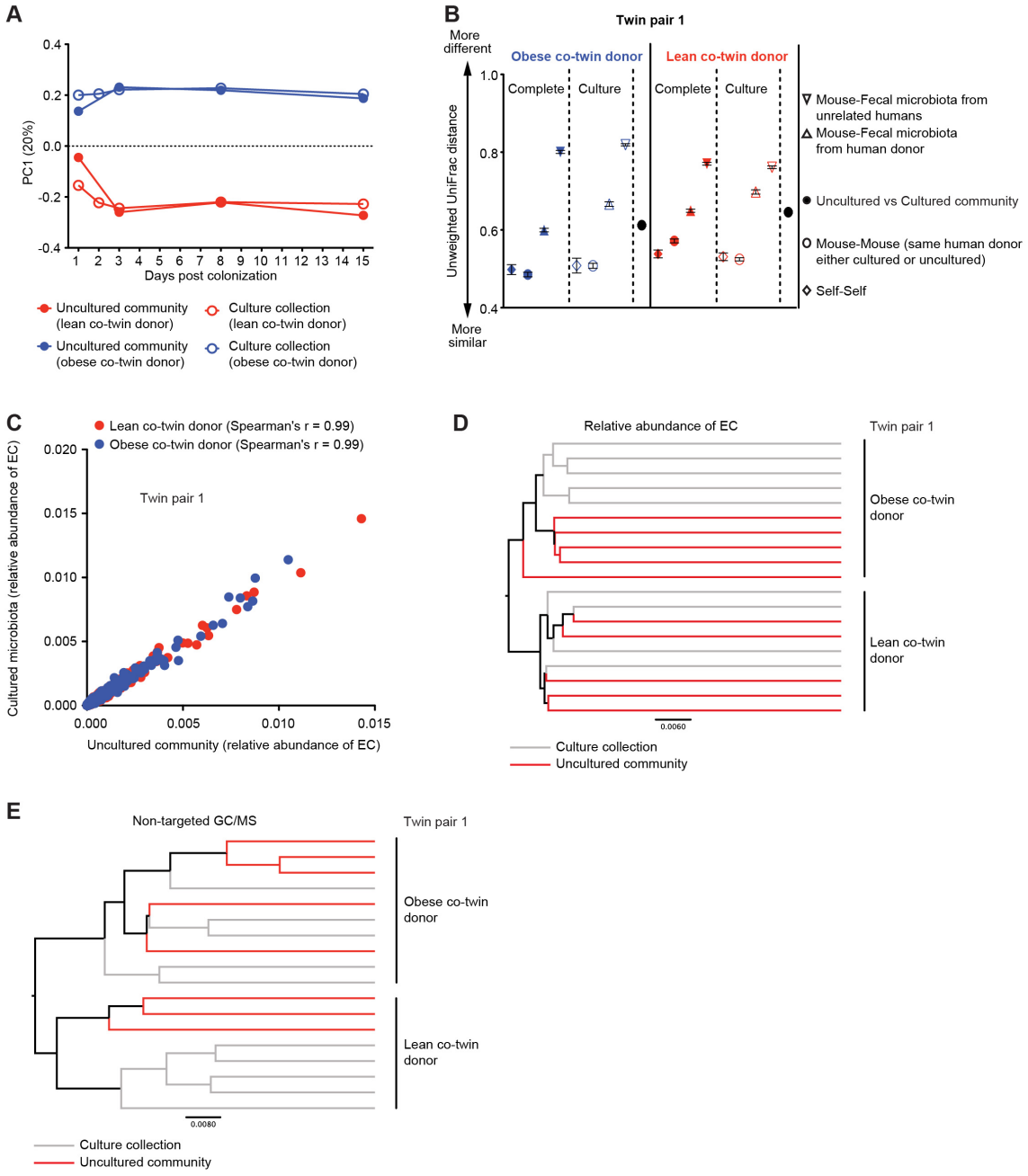

Transplantation of culture collections from the fecal microbiota of co-twins in DZ pair 1 is reproducible within a recipient group of mice and captures interpersonal differences between donors. (A) Assembly of bacterial communities in mice that had received intact uncultured human fecal communities or the corresponding culture collections. PCoA plot based on unweighted UniFrac distance matrix and 97%ID OTUs in sampled fecal communities. Circles correspond to a single mouse fecal sample obtained at a given time point from a given recipient animal. Unfilled circles represent

results obtained from transplantation of intact uncultured communities. Filled circles represent data generated from mice receiving the same donor's culture collection. Circles are colored according to the BMI of the donor. Results from one representative experiment are shown (n=3 independent experiments; 4-5 mice/group). Note that assembly is reproducible within members of a group of mice that have received a given microbiota. **(B)** Mean values ± SEM for pairwise unweighted UniFrac analysis of V2-16S rRNA datasets (97%ID OTUs) are plotted (data shown for 5 mice/treatment group; 4 treatment groups). Color code: filled symbols represent results of pairwise comparisons between recipients of intact uncultured microbiota; unfilled symbols, results of pairwise comparisons between mice harboring culture collections; black circles, pairwise comparison between recipients of intact uncultured microbiota versus the corresponding culture collection. Abbreviations: 'Self-Self', same mouse sampled at different time points within a given experiment; 'Mouse-Mouse', mice colonized with a given donor's fecal microbiota (either intact uncultured sample or the culture collection; 3-8 mice/community type/donor); 'Mouse-Fecal microbiota from human donor', comparison of the fecal microbiota of transplant recipients versus the human donor's microbiota; 'Mouse-Fecal microbiota from unrelated humans', comparison of fecal microbiota from recipients of given donor's microbiota compared to the fecal microbiota of all other unrelated individuals (across twin pair comparison; this latter analysis involved 2 fecal samples obtained two months apart from each individual in each twin pair). **(C)** Correlation between the representation of genes with assigned KEGG EC annotations in the cecal microbiomes of mice harboring a transplanted intact, uncultured community from the obese or lean co-twin from DZ pair 1 versus their representation in the cecal microbiomes of recipients of the corresponding culture collections. Each circle represents an EC. Mean values are plotted for each EC in a given group of mice (n= 4-5 mice/group). Spearman correlation *rho* values are indicated and are significant ($p \leq 0.0001$). **(D)** Unsupervised hierarchical clustering based on a Euclidean dissimilarity matrix calculated from the relative abundance of assigned KEGG ECs in the cecal microbiomes of gnotobiotic recipients of an intact uncultured (red lines) or the corresponding cultured bacterial community (gray lines). **(E)** Hierarchical clustering based on a Euclidean dissimilarity matrix from metabolites identified by nontargeted GC/MS in the cecal contents of mice colonized with intact uncultured (red lines) and cultured (gray lines) gut communities from the co-twins.

Fig. S7

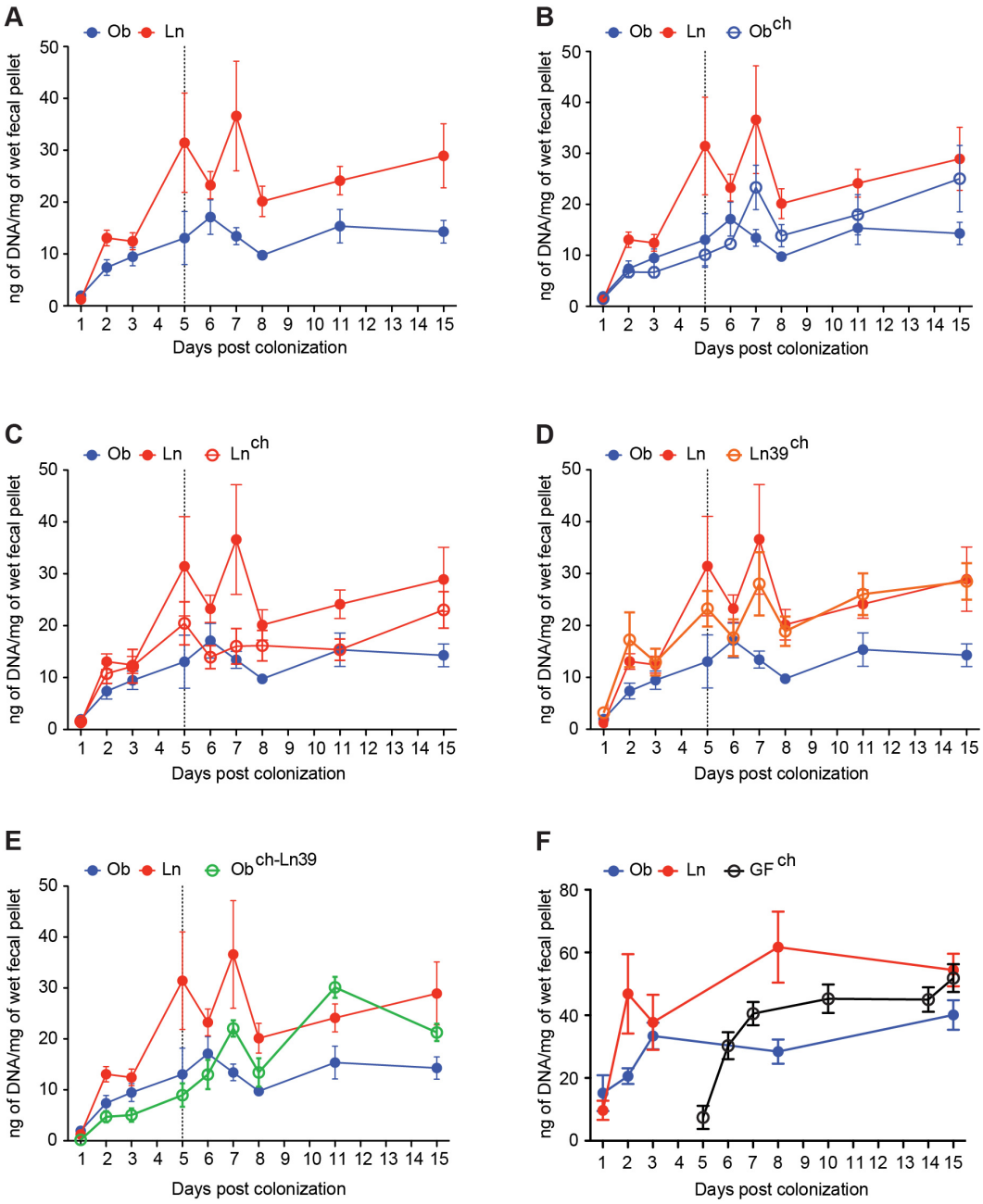

Differences in biomass between fecal samples collected from mice colonized with the cultured microbiota from DZ twin pair 1, discordant for obesity. Biomass was defined as ng DNA/mg wet weight of fecal samples obtained from gnotobiotic mouse recipients of cultured communities prepared from the microbiota of lean (red lines) and obese (blue lines) co-twin donors. **(A)** Ln and Ob controls. **(B)** Ob^{ch} versus Ob and Ln controls **(C)** Ln^{ch} versus Ln and Ob controls, **(D)** $Ln39^{ch}$ versus Ob and Ln controls. **(E)** Ob^{chLn39} versus Ob and Ln controls, **(F)** Germ-free 'bystanders' (GF^{ch}). Mean values ±

SEM are plotted (n=5-6 mice/treatment group; one sample/mouse/time point). The biomass profiles between Ob controls versus Ln, Ln^{ch}, Ob^{ch} and $Ln39^{ch}$ mice are significantly different (two-way ANOVA, $p \leq 0.05$ for panels A-F compared fecal samples collected 6-15 dpc).

Fig. S8

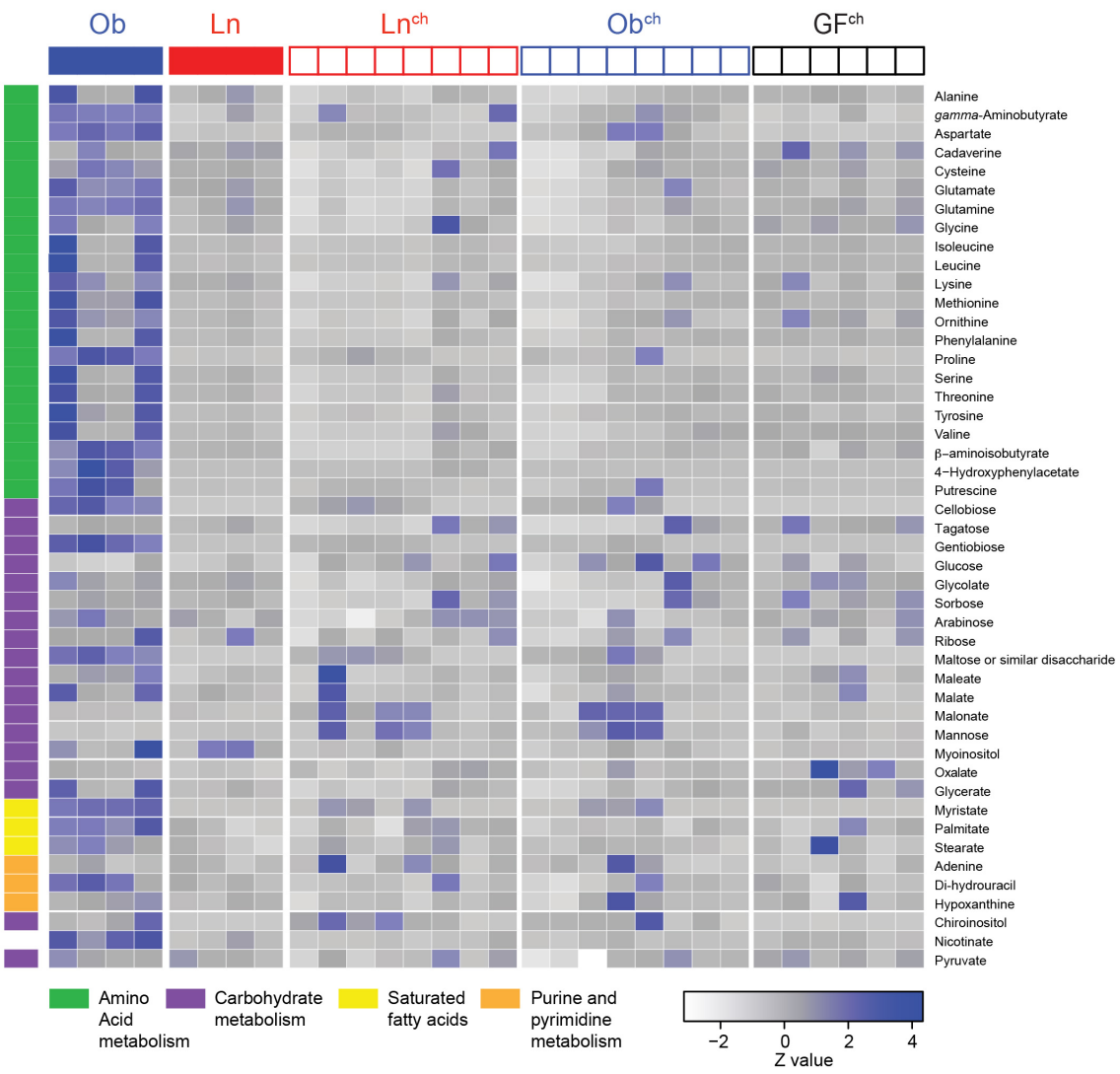

Metabolic profiles generated by nontargeted GC/MS of cecal contents from co-housed mice containing Ln or Ob culture collections and fed a LF/HPP diet. Profiles were subjected to unsupervised hierarchical clustering (Euclidean distance matrix). The heatmap color code shown at the bottom of the panel denotes the relative abundance of a given metabolite normalized across each row. Where groups of co-eluting isomers with similar mass spectra are known to occur, the annotation shown is for the metabolite presumed to be dominant or most likely (*e.g.,* glucose).

Fig. S9

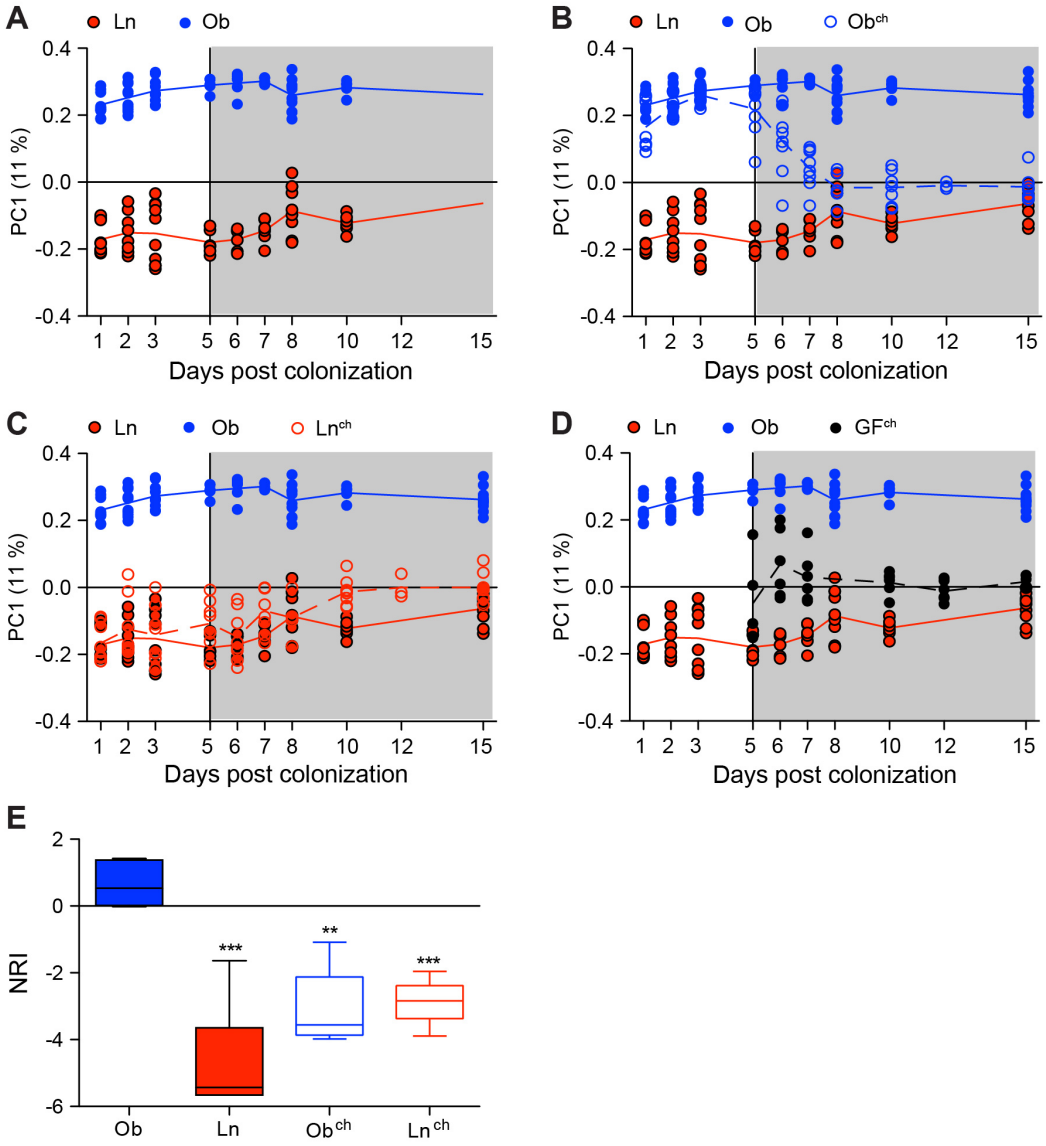

Co-housing gnotobiotic mice fed a LF/HPP diet colonized with the lean co-twin's culture collection transforms the gut community structure of cagemates colonized with her obese co-twin's culture collection to a lean-like state. (A-D) Effect of co-housing on fecal bacterial community structure. Shown are plots of principal coordinate (PC) 1 representing 11% of variance in the dataset, versus time (days post colonization, dpc). The PCoA is based on unweighted UniFrac distance matrix of community 97%ID OTU composition. Each circle represents a microbial community collected from a given mouse at the indicated time point. Colors and symbols describe the culture collection initially introduced into gnotobiotic mouse recipients. Results from two representative experiments are shown. **(E)** Net relatedness index (NRI) calculated based on fecal samples collected 15 d after colonization (10 d after co-housing) from Ln-Ln, Ob-Ob,

Ln^{ch}-Ob^{ch} animals. An asterisk indicates that NRI values were significantly different from zero (** $p \leq 0.01$; *** $p \leq 0.001$, one-sample Student's *t*-test).

Fig. S10

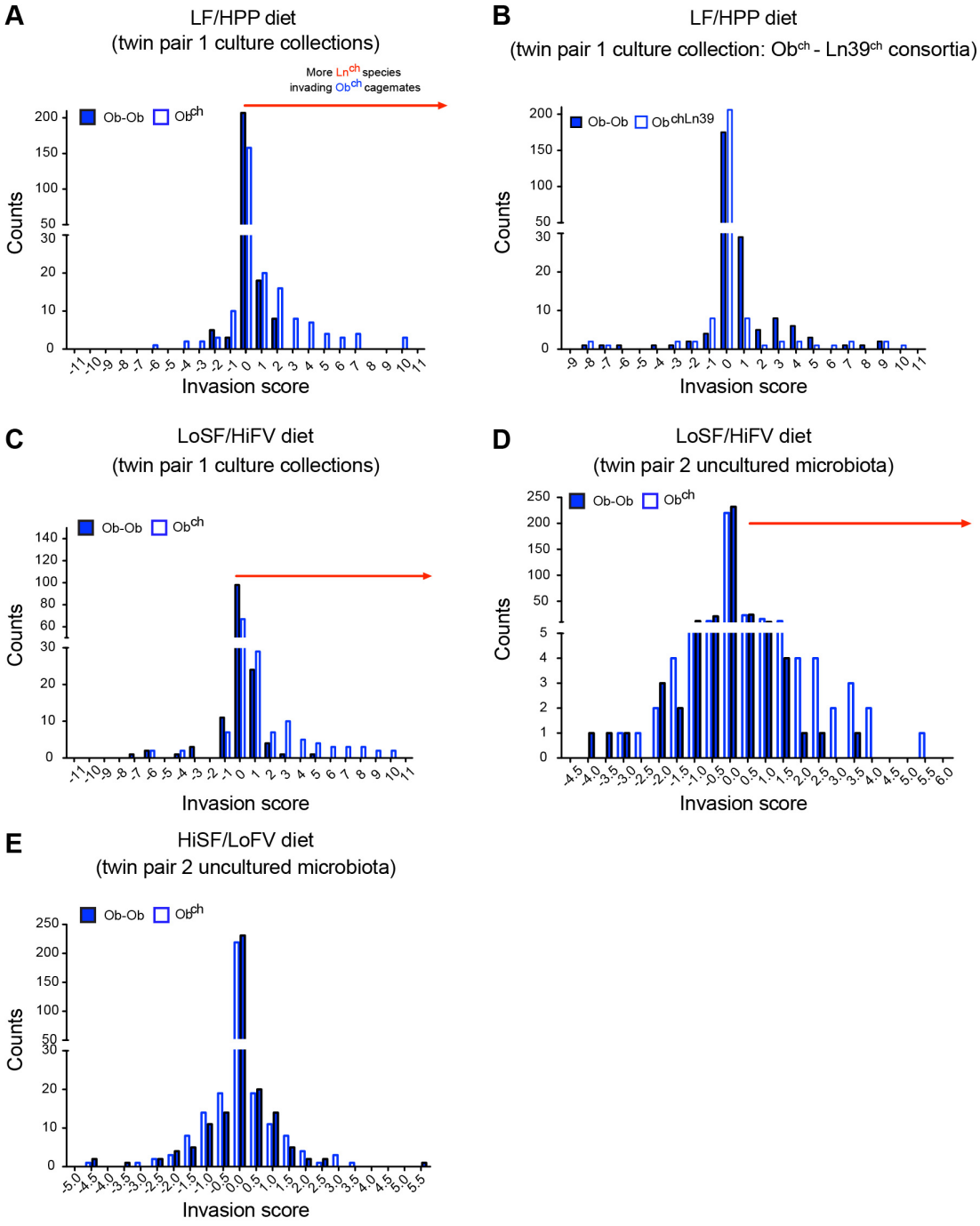

Distribution of invasion scores for the Ob^{ch} microbiota is affected by diet. Histogram of the distribution of invasion scores for dually-housed Ob-Ob controls, or co-housed Ob^{ch} animals that were subjected to five different diet-by-microbiota combinations: **(A)** mice colonized with the Ob culture collection from DZ twin pair 1 co-housed with Ln or **(B)** Ln39 mice and fed a LF/HPP diet; **(C)** mice colonized with the DZ twin pair 1 Ob

culture collection and co-housed with Ln cagemates and fed a LoSF/HiFV diet; **(D)** mice colonized with the intact uncultured fecal microbiota from the obese co-twin in DZ twin pair 2 and co-housed with mice colonized with the intact uncultured fecal microbiota from their lean co-twin and fed a LoSF/HiFV diet or **(E)** the HiSF/LoFV diet. The x-axis shows the invasion scores computed for all gut bacterial taxa observed in members of a given treatment group. The y-axis indicates the number of times (counts) that a particular invasion score was observed in that treatment group. Significant differences between the distributions of invasion scores from the Ob-Ob controls versus Ob^{ch} animals in each treatment group are highlighted by red arrows and defined by a Welch's two-sample *t*-test. The results show that neither Ob^{ch} mice fed a HiSF/LoFV diet (40% fat content by weight), nor Ob^{ch} co-housed with a defined 39-member community, exhibit significant invasion from the microbiota of Ln^{ch} cagemates (significant invasion would have been manifest in this type of plot by a significant shift in the distribution of invasion scores to more positive values).

Fig. S11

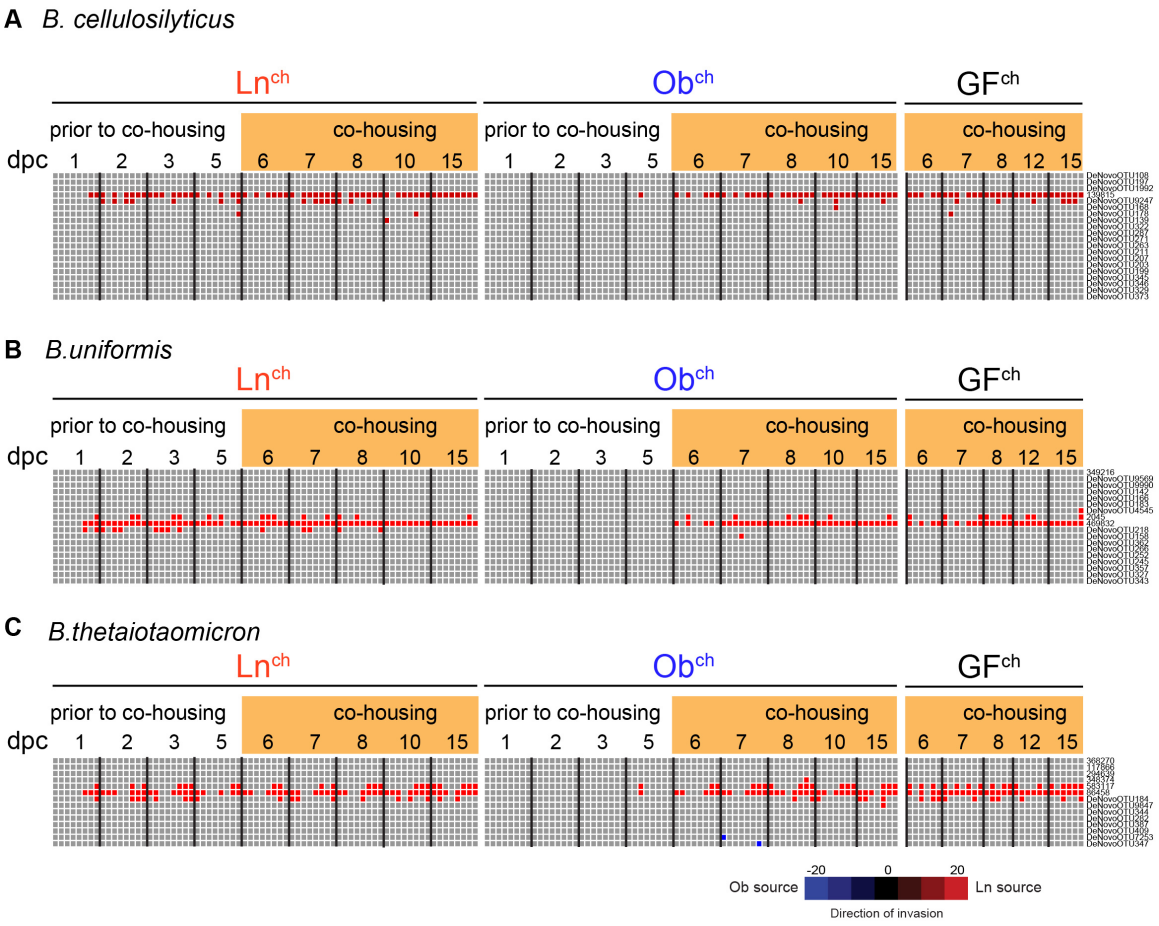

SourceTracker demonstrates the specificity of invasion at the level of 97%ID OTUs in co-housed Ln, Ob, and GF mice consuming the LF/HPP diet. Each row represents a 97%ID OTU assigned to the species indicated at the top of each panel. OTU identification numbers are provided at the end of each row for reference. **dpc**, days post colonization. The direction of invasion of OTUs belonging to **(A)** *Bacteroides cellulosilyticus*, **(B)** *Bacteroides uniformis,* and **(C)** *Bacteroides thetaiotaomicron* is shown (all from Ln^{ch} to Ob^{ch}).

Fig. S12

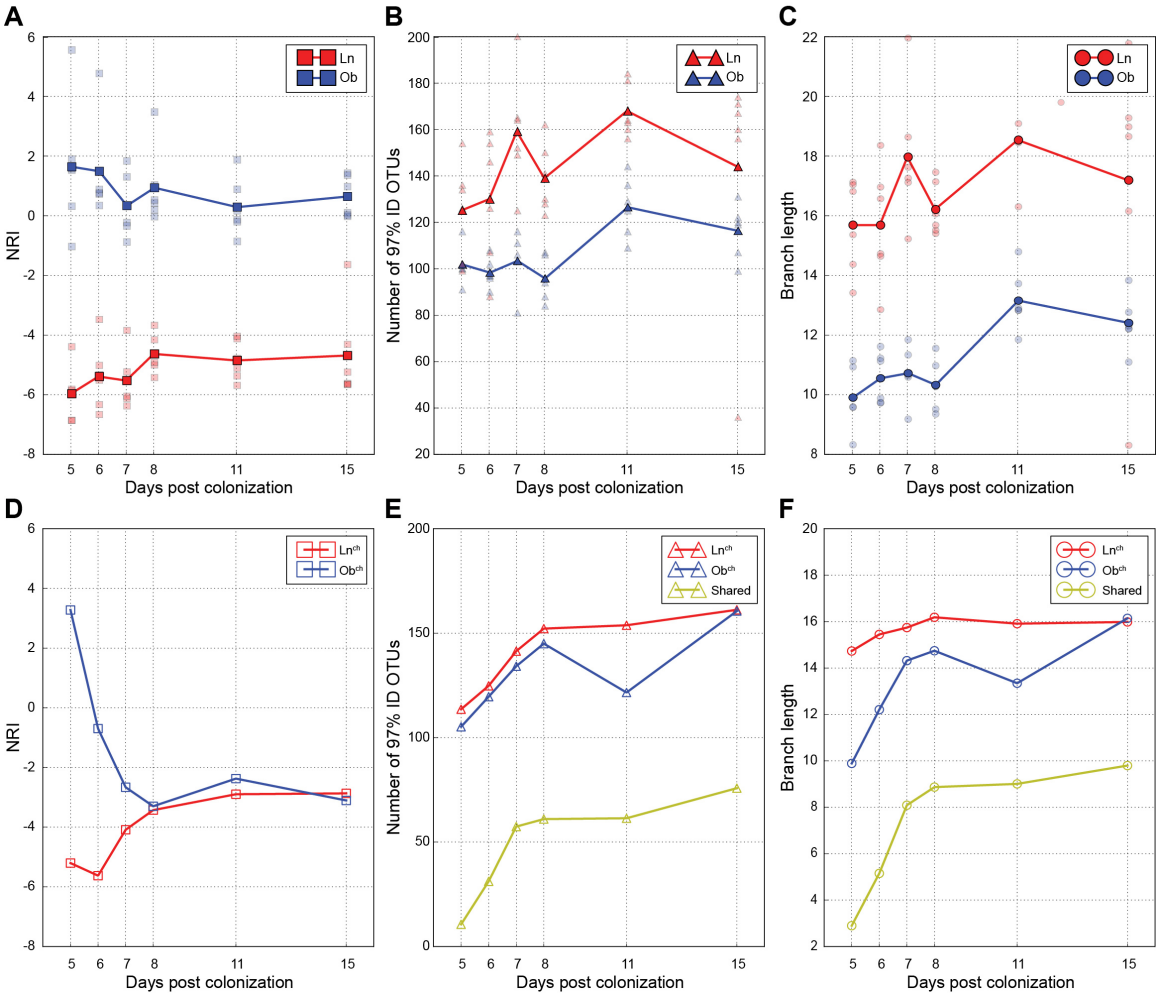

Changes in phylogenetic structure of invaded Ob^{ch} communities. Red lines and red symbols represent mice consuming a LF/HPP diet that were originally colonized with a culture collection from the lean co-twin in DZ pair 1 (Ln). Blue lines and blue symbols represent mice that received a culture collection from her obese co-twin (Ob). Closed symbols represent dually-housed Ln-Ln or Ob-Ob controls. Open symbols represent co-housed Ob^{ch} and Ln^{ch} cagemates. Light green lines represent the number of shared 97%ID OTUs, or branch length, in panels B-E. **(A)** Net Relatedness Index (NRI), **(B)** number of 97%ID OTUs and **(C)** branch length were calculated for Ln and Ob controls. Unlike with Ob-Ob controls, the NRI for Ln-Ln controls was significantly different from zero for the duration of the experiment, suggesting a non-random phylogenetic over-dispersion of their community ($p \leq 0.05$, one-sample *t*-test). Moreover, Ln-Ln and Ob-Ob controls had significantly different NRI scores ($p \leq 0.05$; significant interaction by two-way ANOVA with Dunnett's correction for multiple hypothesis). In addition, Ln-Ln controls had significantly greater number of 97%ID OTUs and branch length than Ob-Ob controls ($p \leq 0.05$; two-way ANOVA with Dunnett's correction for multiple hypothesis). **(D)** NRI, **(E)** number of 97%ID OTUs and **(F)** branch length calculated for Ln^{ch} and Ob^{ch} cagemates. NRI for Ob^{ch} animals was not significantly different from that of Ln^{ch}

cagemates 10 d after co-housing ($p \leq 0.05$, paired Student's *t*-test). The number of shared 97%ID OTUs as well as the shared branch length between Ob^{ch} and Ln^{ch} cagemates was significantly higher 10 d after co-housing compared to the beginning of the co-housing period ($p \leq 0.0001$, paired Student's *t*-test).

Fig. S13

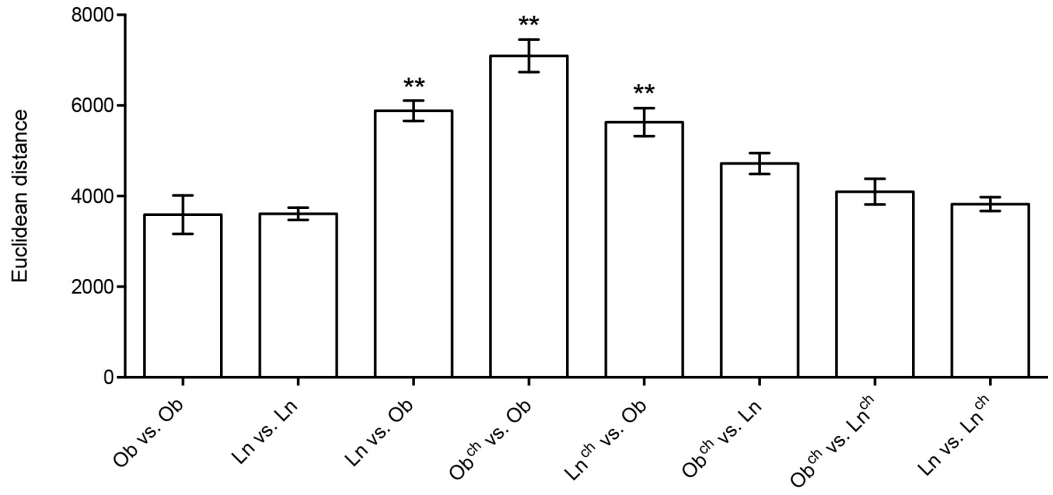

Global changes in the cecal meta-transcriptomes of Ob^{ch} animals fed the LF/HPP diet. Cecal samples collected at the time of sacrifice from Ln^{ch}, Ob^{ch} and control animals were subjected to microbial RNA-Seq. A total of 23,032,985 ± 16,990,559 reads/sample (mean ± SD) were mapped to the sequenced genomes of 148 bacterial taxa isolated from the human gut: 16.3 ± 6.5% (mean ±SD) of the reads mapped to known or predicted proteins in these genomes; 60.1 ± 1.3 % of these mapped reads were assigned to ECs (KEGG version 58). Euclidian distances were calculated using reads that mapped to ECs. Distances between the indicated comparisons that are significantly dissimilar to the distances between reference co-housed Ob-Ob controls are indicated with asterisks (** $p \leq 0.001$, as measured by a one-way ANOVA, with Holm- Šidák's correction for multiple hypotheses).

Fig. S14

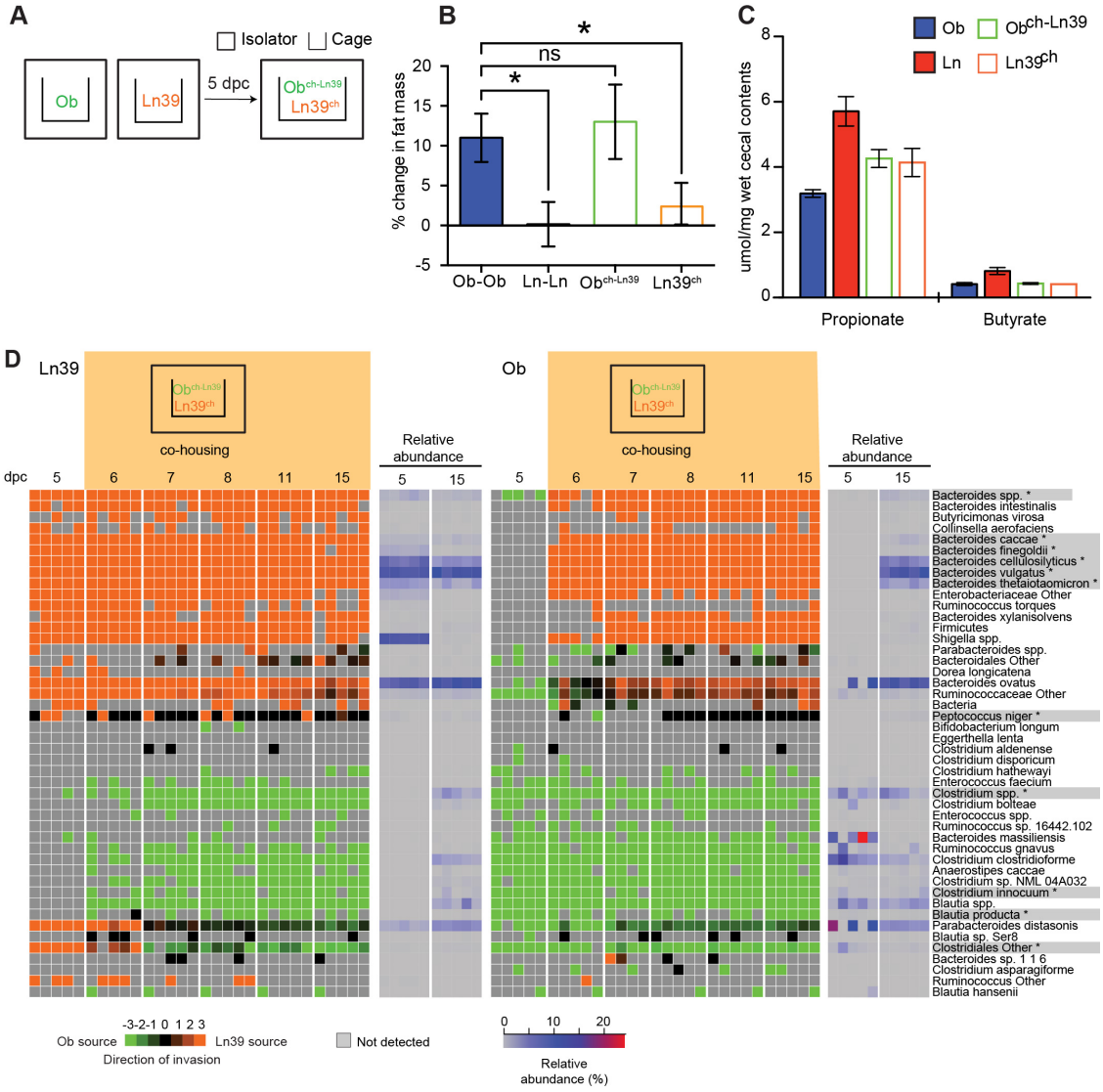

Co-housing experiment involving mice colonized with the obese co-twin's culture collection and mice colonized with a consortium of 39 sequenced bacteria taxa from an arrayed culture collection generated from the lean co-twin. Mice were fed the LF/HPP diet. **(A)** 'Reference controls' consisted of co-housed Ln-Ln, Ob-Ob animals, while the experimental group consisted of Ob mice co-housed with mice that had received a consortia of 39 strains from the clonally-arrayed, taxonomically defined Ln culture collection (Ln39) (n= 5 cages/experiment; 2 independent experiments). **(B,C)** $Ln39^{ch}$ mice were not able to ameliorate the adiposity phenotype (panel B), nor did they increase cecal SCFA concentrations in $Ob^{ch\text{-}Ln39}$ cagemates (panel C; one-tailed, unpaired Student's *t*-test; * $p \leq 0.05$). **(D)** Invasion analysis of species-level taxa based on log odds

ratio between invasive species belonging to Ob^{ch} or $Ln39^{ch}$ mice before and after co-housing. Orange denotes invasive species-level taxa originating from $Ln39^{ch}$ mice. Green indicates invasive species-level taxa originating from $Ob^{ch\text{-}Ln39}$ animals. The relative abundance of each species-level taxon before (5 dpc) and after (15 dpc) co-housing is indicated. Results shown are from one representative experiment.

Fig. S15

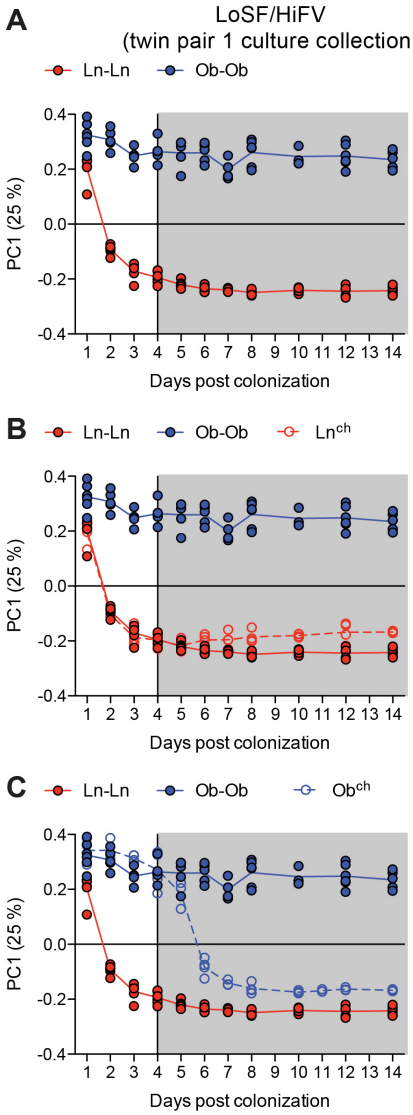

Co-housing gnotobiotic mice fed the NHANES-based LoSF/HiFV diet that are colonized with the lean co-twin's culture collection transforms the gut community structure of cagemates colonized with her obese co-twin's culture collection to a lean-like state. (**A-C**) Effect of co-housing on fecal bacterial community structure. Plots of principal coordinate (PC) 1 representing 25% of variance in the dataset versus time (days post colonization, dpc). The plot was generated using an unweighted UniFrac distance matrix of community 97%ID OTU composition. Each circle represents a microbial community collected from a given mouse sampled at the indicated time point. Colors and symbols describe the culture collection initially introduced into gnotobiotic mouse recipients.

Fig. S16

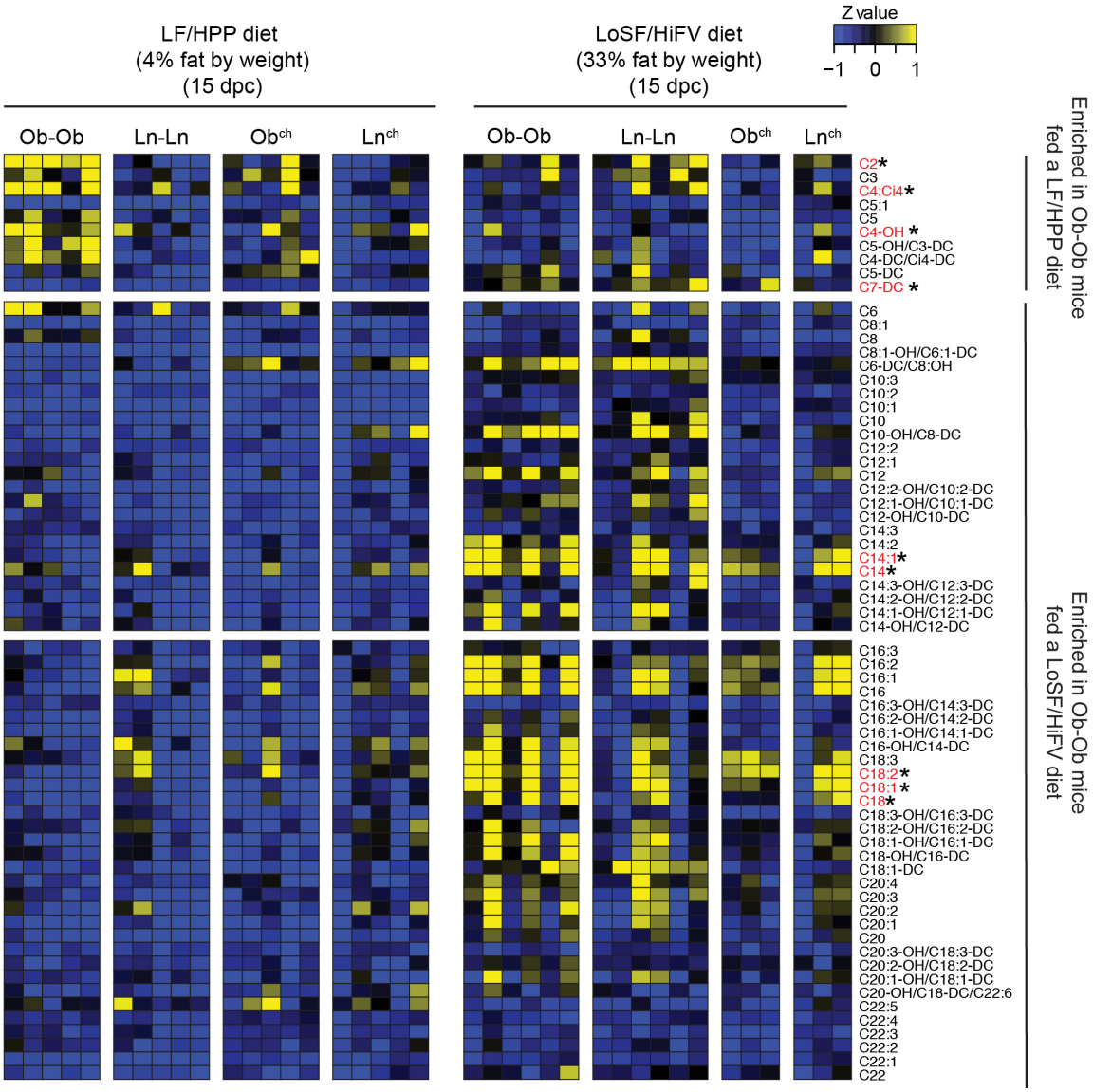

Acylcarnitine profiles of liver samples collected from mice colonized with the culture collections from Ln or Ob co-twins from DZ twin pair 1 and fed either the LF/HPP or LoSF/HiFV diets. Each column represents a different animal and each row a different acylcarnitine. The identities and levels of these acylcarnitines were determined by targeted MS/MS (see **table S15** for mean values ± SEM for each treatment group). * $p < 0.05$. A two-way ANOVA with Holm- Šidák's correction was used to calculate whether the level of each acylcarnitine was significantly different between Ob-Ob versus Ln-Ln, Ln^{ch} or Ob^{ch} animals. * $p \leq 0.05$.

Fig. S17

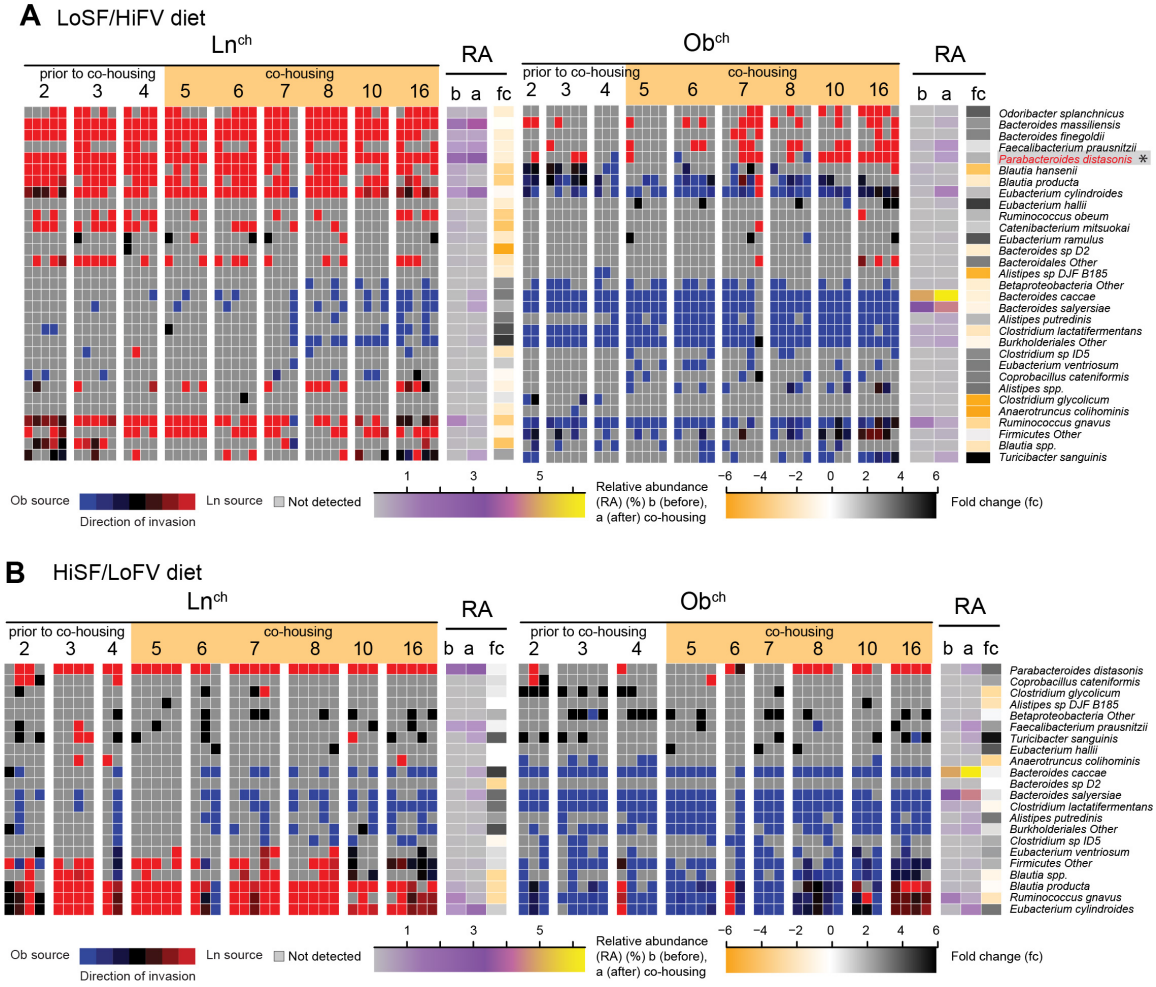

Invasion analysis from co-housing experiments involving mice with either the obese or lean co-twin's uncultured fecal microbiota from DZ twin pair 2 and fed one of two NHANES-based diets. Invasion analysis of species-level taxa was based on log odds ratio between species belonging to Ob^{ch} or Ln^{ch} mice before and after co-housing. Red denotes invasive species-level bacterial taxa originating from Ln^{ch} cagemates, while blue indicates invasive species-level taxa originating from Ob^{ch} animals. The relative abundance of each species-level taxon before [**b**, 5 days post colonization (dpc)] and after (**a**, 15 dpc) co-housing is indicated. The fold-change (fc) in relative abundance before and after co-housing is shown (see legend to Fig. 2E).

References and Notes

1. P. B. Eckburg, E. M. Bik, C. N. Bernstein, E. Purdom, L. Dethlefsen, M. Sargent, S. R. Gill, K. E. Nelson, D. A. Relman, Diversity of the human intestinal microbial flora. *Science* **308**, 1635–1638 (2005). doi:10.1126/science.1110591

2. P. J. Turnbaugh, M. Hamady, T. Yatsunenko, B. L. Cantarel, A. Duncan, R. E. Ley, M. L. Sogin, W. J. Jones, B. A. Roe, J. P. Affourtit, M. Egholm, B. Henrissat, A. C. Heath, R. Knight, J. I. Gordon, A core gut microbiome in obese and lean twins. *Nature* **457**, 480–484 (2009). Medline doi:10.1038/nature07540

3. E. K. Costello, C. L. Lauber, M. Hamady, N. Fierer, J. I. Gordon, R. Knight, Bacterial community variation in human body habitats across space and time. *Science* **326**, 1694–1697 (2009). doi:10.1126/science.1177486

4. J. Qin, R. Li, J. Raes, M. Arumugam, K. S. Burgdorf, C. Manichanh, T. Nielsen, N. Pons, F. Levenez, T. Yamada, D. R. Mende, J. Li, J. Xu, S. Li, D. Li, J. Cao, B. Wang, H. Liang, H. Zheng, Y. Xie, J. Tap, P. Lepage, M. Bertalan, J. M. Batto, T. Hansen, D. Le Paslier, A. Linneberg, H. B. Nielsen, E. Pelletier, P. Renault, T. Sicheritz-Ponten, K. Turner, H. Zhu, C. Yu, S. Li, M. Jian, Y. Zhou, Y. Li, X. Zhang, S. Li, N. Qin, H. Yang, J. Wang, S. Brunak, J. Doré, F. Guarner, K. Kristiansen, O. Pedersen, J. Parkhill, J. Weissenbach, MetaHIT Consortium, P. Bork, S. D. Ehrlich, J. Wang, A human gut microbial gene catalogue established by metagenomic sequencing. *Nature* **464**, 59–65 (2010). Medline doi:10.1038/nature08821

5. J. Ravel, P. Gajer, Z. Abdo, G. M. Schneider, S. S. Koenig, S. L. McCulle, S. Karlebach, R. Gorle, J. Russell, C. O. Tacket, R. M. Brotman, C. C. Davis, K. Ault, L. Peralta, L. J. Forney, Vaginal microbiome of reproductive-age women. *Proc. Natl. Acad. Sci. U.S.A.* **108**(Suppl. 1), 4680–4687 (2011). Medline doi:10.1073/pnas.1002611107

6. P. Gajer, R. M. Brotman, G. Bai, J. Sakamoto, U. M. Schütte, X. Zhong, S. S. Koenig, L. Fu, Z. S. Ma, X. Zhou, Z. Abdo, L. J. Forney, J. Ravel, Temporal dynamics of the human vaginal microbiota. *Sci. Transl. Med.* **4**, 32ra52 (2012).doi:10.1126/scitranslmed.3003605

7. T. Yatsunenko, F. E. Rey, M. J. Manary, I. Trehan, M. G. Dominguez-Bello, M. Contreras, M. Magris, G. Hidalgo, R. N. Baldassano, A. P. Anokhin, A. C. Heath, B. Warner, J. Reeder, J. Kuczynski, J. G. Caporaso, C. A. Lozupone, C. Lauber, J. C. Clemente, D. Knights, R. Knight, J. I. Gordon, Human gut microbiome viewed across age and geography. *Nature* **486**, 222–227 (2012). Medline

8. C. Huttenhower, D. Gevers, R. Knight, S. Abubucker, J. H. Badger, A. T. Chinwalla, H. H. Creasy, A. M. Earl, M. G. FitzGerald, R. S. Fulton, M. G. Giglio, K. Hallsworth-Pepin, E. A. Lobos, R. Madupu, V. Magrini, J. C. Martin, M. Mitreva, D. M. Muzny, E. J. Sodergren, J. Versalovic, A. M. Wollam, K. C. Worley, J. R. Wortman, S. K. Young, Q. Zeng, K. M. Aagaard, O. O. Abolude, E. Allen-Vercoe, E. J. Alm, L. Alvarado, G. L. Andersen, S. Anderson, E. Appelbaum, H. M. Arachchi, G. Armitage, C. A. Arze, T. Ayvaz, C. C. Baker, L. Begg, T. Belachew, V. Bhonagiri, M. Bihan, M. J. Blaser, T. Bloom, V. Bonazzi, J. Paul

Brooks, G. A. Buck, C. J. Buhay, D. A. Busam, J. L. Campbell, S. R. Canon, B. L. Cantarel, P. S. G. Chain, I.-M. A. Chen, L. Chen, S. Chhibba, K. Chu, D. M. Ciulla, J. C. Clemente, S. W. Clifton, S. Conlan, J. Crabtree, M. A. Cutting, N. J. Davidovics, C. C. Davis, T. Z. DeSantis, C. Deal, K. D. Delehaunty, F. E. Dewhirst, E. Deych, Y. Ding, D. J. Dooling, S. P. Dugan, W. Michael Dunne, A. Scott Durkin, R. C. Edgar, R. L. Erlich, C. N. Farmer, R. M. Farrell, K. Faust, M. Feldgarden, V. M. Felix, S. Fisher, A. A. Fodor, L. J. Forney, L. Foster, V. Di Francesco, J. Friedman, D. C. Friedrich, C. C. Fronick, L. L. Fulton, H. Gao, N. Garcia, G. Giannoukos, C. Giblin, M. Y. Giovanni, J. M. Goldberg, J. Goll, A. Gonzalez, A. Griggs, S. Gujja, S. Kinder Haake, B. J. Haas, H. A. Hamilton, E. L. Harris, T. A. Hepburn, B. Herter, D. E. Hoffmann, M. E. Holder, C. Howarth, K. H. Huang, S. M. Huse, J. Izard, J. K. Jansson, H. Jiang, C. Jordan, V. Joshi, J. A. Katancik, W. A. Keitel, S. T. Kelley, C. Kells, N. B. King, D. Knights, H. H. Kong, O. Koren, S. Koren, K. C. Kota, C. L. Kovar, N. C. Kyrpides, P. S. La Rosa, S. L. Lee, K. P. Lemon, N. Lennon, C. M. Lewis, L. Lewis, R. E. Ley, K. Li, K. Liolios, B. Liu, Y. Liu, C.-C. Lo, C. A. Lozupone, R. Dwayne Lunsford, T. Madden, A. A. Mahurkar, P. J. Mannon, E. R. Mardis, V. M. Markowitz, K. Mavromatis, J. M. McCorrison, D. McDonald, J. McEwen, A. L. McGuire, P. McInnes, T. Mehta, K. A. Mihindukulasuriya, J. R. Miller, P. J. Minx, I. Newsham, C. Nusbaum, M. O'Laughlin, J. Orvis, I. Pagani, K. Palaniappan, S. M. Patel, M. Pearson, J. Peterson, M. Podar, C. Pohl, K. S. Pollard, M. Pop, M. E. Priest, L. M. Proctor, X. Qin, J. Raes, J. Ravel, J. G. Reid, M. Rho, R. Rhodes, K. P. Riehle, M. C. Rivera, B. Rodriguez-Mueller, Y.-H. Rogers, M. C. Ross, C. Russ, R. K. Sanka, P. Sankar, J. Fah Sathirapongsasuti, J. A. Schloss, P. D. Schloss, T. M. Schmidt, M. Scholz, L. Schriml, A. M. Schubert, N. Segata, J. A. Segre, W. D. Shannon, R. R. Sharp, T. J. Sharpton, N. Shenoy, N. U. Sheth, G. A. Simone, I. Singh, C. S. Smillie, J. D. Sobel, D. D. Sommer, P. Spicer, G. G. Sutton, S. M. Sykes, D. G. Tabbaa, M. Thiagarajan, C. M. Tomlinson, M. Torralba, T. J. Treangen, R. M. Truty, T. A. Vishnivetskaya, J. Walker, L. Wang, Z. Wang, D. V. Ward, W. Warren, M. A. Watson, C. Wellington, K. A. Wetterstrand, J. R. White, K. Wilczek-Boney, Y. Q. Wu, K. M. Wylie, T. Wylie, C. Yandava, L. Ye, Y. Ye, S. Yooseph, B. P. Youmans, L. Zhang, Y. Zhou, Y. Zhu, L. Zoloth, J. D. Zucker, B. W. Birren, R. A. Gibbs, S. K. Highlander, B. A. Methé, K. E. Nelson, J. F. Petrosino, G. M. Weinstock, R. K. Wilson, O. White, Structure, function and diversity of the healthy human microbiome. *Nature* **486**, 207–214 (2012). Medline doi:10.1038/nature11234

9. K. Faust, J. F. Sathirapongsasuti, J. Izard, N. Segata, D. Gevers, J. Raes, C. Huttenhower, Microbial co-occurrence relationships in the human microbiome. *PLOS Comput. Biol.* **8**, e1002606 (2012). Medline doi:10.1371/journal.pcbi.1002606

10. M. G. Dominguez-Bello, E. K. Costello, M. Contreras, M. Magris, G. Hidalgo, N. Fierer, R. Knight, Delivery mode shapes the acquisition and structure of the initial microbiota across multiple body habitats in newborns. *Proc. Natl. Acad. Sci. U.S.A.* **107**, 11971–11975 (2010). Medline doi:10.1073/pnas.1002601107

11. J. E. Koenig, A. Spor, N. Scalfone, A. D. Fricker, J. Stombaugh, R. Knight, L. T. Angenent, R. E. Ley, Succession of microbial consortia in the developing infant gut microbiome. *Proc. Natl. Acad. Sci. U.S.A.* **108**(Suppl. 1), 4578–4585 (2011). Medline doi:10.1073/pnas.1000081107

12. S. Greenblum, P. J. Turnbaugh, E. Borenstein, Metagenomic systems biology of the human gut microbiome reveals topological shifts associated with obesity and inflammatory bowel disease. *Proc. Natl. Acad. Sci. U.S.A.* **109**, 594–599 (2012). Medline doi:10.1073/pnas.1116053109

13. M. L. Zupancic, B. L. Cantarel, Z. Liu, E. F. Drabek, K. A. Ryan, S. Cirimotich, C. Jones, R. Knight, W. A. Walters, D. Knights, E. F. Mongodin, R. B. Horenstein, B. D. Mitchell, N. Steinle, S. Snitker, A. R. Shuldiner, C. M. Fraser, Analysis of the gut microbiota in the old order Amish and its relation to the metabolic syndrome. *PLoS ONE* **7**, e43052 (2012). Medline doi:10.1371/journal.pone.0043052

14. S. H. Duncan, G. E. Lobley, G. Holtrop, J. Ince, A. M. Johnstone, P. Louis, H. J. Flint, Human colonic microbiota associated with diet, obesity and weight loss. *Int J Obes (Lond)* **32**, 1720–1724 (2008). Medline doi:10.1038/ijo.2008.155

15. A. Schwiertz, D. Taras, K. Schäfer, S. Beijer, N. A. Bos, C. Donus, P. D. Hardt, Microbiota and SCFA in lean and overweight healthy subjects. *Obesity (Silver Spring)* **18**, 190–195 (2010). Medline doi:10.1038/oby.2009.167

16. A. Santacruz, M. C. Collado, L. García-Valdés, M. T. Segura, J. A. Martín-Lagos, T. Anjos, M. Martí-Romero, R. M. Lopez, J. Florido, C. Campoy, Y. Sanz, Gut microbiota composition is associated with body weight, weight gain and biochemical parameters in pregnant women. *Br. J. Nutr.* **104**, 83–92 (2010). Medline doi:10.1017/S0007114510000176

17. R. Jumpertz, D. S. Le, P. J. Turnbaugh, C. Trinidad, C. Bogardus, J. I. Gordon, J. Krakoff, Energy-balance studies reveal associations between gut microbes, caloric load, and nutrient absorption in humans. *Am. J. Clin. Nutr.* **94**, 58–65 (2011). Medline doi:10.3945/ajcn.110.010132

18. A. Vrieze, E. Van Nood, F. Holleman, J. Salojärvi, R. S. Kootte, J. F. Bartelsman, G. M. Dallinga-Thie, M. T. Ackermans, M. J. Serlie, R. Oozeer, M. Derrien, A. Druesne, J. E. Van Hylckama Vlieg, V. W. Bloks, A. K. Groen, H. G. Heilig, E. G. Zoetendal, E. S. Stroes, W. M. de Vos, J. B. Hoekstra, M. Nieuwdorp, Transfer of intestinal microbiota from lean donors increases insulin sensitivity in individuals with metabolic syndrome. *Gastroenterology* **143**, 913, e7 (2012). Medline doi:10.1053/j.gastro.2012.06.031

19. P. Hakala, A. Rissanen, M. Koskenvuo, J. Kaprio, T. Rönnemaa, Environmental factors in the development of obesity in identical twins. *Int. J. Obes. Relat. Metab. Disord.* **23**, 746–753 (1999). Medline doi:10.1038/sj.ijo.0800923

20. A. Rissanen, P. Hakala, L. Lissner, C. E. Mattlar, M. Koskenvuo, T. Rönnemaa, Acquired preference especially for dietary fat and obesity: A study of weight-discordant monozygotic twin pairs. *Int. J. Obes. Relat. Metab. Disord.* **26**, 973–977 (2002). Medline

21. A. E. Duncan, A. Agrawal, J. D. Grant, K. K. Bucholz, P. A. Madden, A. C. Heath, Genetic and environmental contributions to BMI in adolescent and young adult women. *Obesity (Silver Spring)* **17**, 1040–1043 (2009). Medline doi:10.1038/oby.2008.643

22. M. Waldron, K. K. Bucholz, M. T. Lynskey, P. A. Madden, A. C. Heath, Alcoholism and timing of separation in parents: Findings in a midwestern birth cohort. *J. Stud. Alcohol Drugs* **74**, 337–348 (2013). Medline

23. Materials and methods are available as supplementary material on *Science* Online.

24. E. Kristiansson, P. Hugenholtz, D. Dalevi, ShotgunFunctionalizeR: An R-package for functional comparison of metagenomes. *Bioinformatics* **25**, 2737–2738 (2009). Medline doi:10.1093/bioinformatics/btp508

25. C. B. Newgard, J. An, J. R. Bain, M. J. Muehlbauer, R. D. Stevens, L. F. Lien, A. M. Haqq, S. H. Shah, M. Arlotto, C. A. Slentz, J. Rochon, D. Gallup, O. Ilkayeva, B. R. Wenner, W. S. Yancy Jr., H. Eisenson, G. Musante, R. S. Surwit, D. S. Millington, M. D. Butler, L. P. Svetkey, A branched-chain amino acid-related metabolic signature that differentiates obese and lean humans and contributes to insulin resistance. *Cell Metab.* **9**, 311–326 (2009). Medline doi:10.1016/j.cmet.2009.02.002

26. B. D. Muegge, J. Kuczynski, D. Knights, J. C. Clemente, A. González, L. Fontana, B. Henrissat, R. Knight, J. I. Gordon, Diet drives convergence in gut microbiome functions across mammalian phylogeny and within humans. *Science* **332**, 970–974 (2011). doi:10.1126/science.1198719

27. M. J. Keenan, J. Zhou, K. L. McCutcheon, A. M. Raggio, H. G. Bateman, E. Todd, C. K. Jones, R. T. Tulley, S. Melton, R. J. Martin, M. Hegsted, Effects of resistant starch, a non-digestible fermentable fiber, on reducing body fat. *Obesity (Silver Spring)* **14**, 1523–1534 (2006). Medline doi:10.1038/oby.2006.176

28. J. Zhou, R. J. Martin, R. T. Tulley, A. M. Raggio, K. L. McCutcheon, L. Shen, S. C. Danna, S. Tripathy, M. Hegsted, M. J. Keenan, Dietary resistant starch upregulates total GLP-1 and PYY in a sustained day-long manner through fermentation in rodents. *Am. J. Physiol. Endocrinol. Metab.* **295**, E1160–E1166 (2008). Medline doi:10.1152/ajpendo.90637.2008

29. J. Zhou, R. J. Martin, R. T. Tulley, A. M. Raggio, L. Shen, E. Lissy, K. McCutcheon, M. J. Keenan, Failure to ferment dietary resistant starch in specific mouse models of obesity results in no body fat loss. *J. Agric. Food Chem.* **57**, 8844–8851 (2009). Medline doi:10.1021/jf901548e

30. D. Knights, J. Kuczynski, E. S. Charlson, J. Zaneveld, M. C. Mozer, R. G. Collman, F. D. Bushman, R. Knight, S. T. Kelley, Bayesian community-wide culture-independent microbial source tracking. *Nat. Methods* **8**, 761–763 (2011). Medline doi:10.1038/nmeth.1650

31. J. P. Lessard, J. A. Fordyce, N. J. Gotelli, N. J. Sanders, Invasive ants alter the phylogenetic structure of ant communities. *Ecology* **90**, 2664–2669 (2009). Medline doi:10.1890/09-0503.1

32. M. T. Johnson, J. R. Stinchcombe, An emerging synthesis between community ecology and evolutionary biology. *Trends Ecol. Evol.* **22**, 250–257 (2007). Medline doi:10.1016/j.tree.2007.01.014

33. C. O. Webb, N. C. Pitman, Phylogenetic balance and ecological evenness. *Syst. Biol.* **51**, 898–907 (2002). Medline doi:10.1080/10635150290102609

[BPO1]34. P. J. Turnbaugh, R. E. Ley, M. A. Mahowald, V. Magrini, E. R. Mardis, J. I. Gordon, An obesity-associated gut microbiome with increased capacity for energy harvest. *Nature* **444**, 1027–1031 (2006). Medline doi:10.1038/nature05414

35. P. Gauffin Cano, A. Santacruz, A. Moya, Y. Sanz, Bacteroides uniformis CECT 7771 ameliorates metabolic and immunological dysfunction in mice with high-fat-diet induced obesity. *PLoS ONE* **7**, e41079 (2012). Medline doi:10.1371/journal.pone.0041079

36. S. H. Duncan, G. Holtrop, G. E. Lobley, A. G. Calder, C. S. Stewart, H. J. Flint, Contribution of acetate to butyrate formation by human faecal bacteria. *Br. J. Nutr.* **91**, 915–923 (2004). Medline doi:10.1079/BJN20041150

37. M. A. Mahowald, F. E. Rey, H. Seedorf, P. J. Turnbaugh, R. S. Fulton, A. Wollam, N. Shah, C. Wang, V. Magrini, R. K. Wilson, B. L. Cantarel, P. M. Coutinho, B. Henrissat, L. W. Crock, A. Russell, N. C. Verberkmoes, R. L. Hettich, J. I. Gordon, Characterizing a model human gut microbiota composed of members of its two dominant bacterial phyla. *Proc. Natl. Acad. Sci. U.S.A.* **106**, 5859–5864 (2009). Medline doi:10.1073/pnas.0901529106

38. Z. Gao, J. Yin, J. Zhang, R. E. Ward, R. J. Martin, M. Lefevre, W. T. Cefalu, J. Ye, Butyrate improves insulin sensitivity and increases energy expenditure in mice. *Diabetes* **58**, 1509–1517 (2009). Medline doi:10.2337/db08-1637

39. H. V. Lin, A. Frassetto, E. J. Kowalik Jr., A. R. Nawrocki, M. M. Lu, J. R. Kosinski, J. A. Hubert, D. Szeto, X. Yao, G. Forrest, D. J. Marsh, Butyrate and propionate protect against diet-induced obesity and regulate gut hormones via free fatty acid receptor 3-independent mechanisms. *PLoS ONE* **7**, e35240 (2012). Medline doi:10.1371/journal.pone.0035240

40. H. Kuribayashi, M. Miyata, H. Yamakawa, K. Yoshinari, Y. Yamazoe, Enterobacteria-mediated deconjugation of taurocholic acid enhances ileal farnesoid X receptor signaling. *Eur. J. Pharmacol.* **697**, 132–138 (2012). Medline doi:10.1016/j.ejphar.2012.09.048

41. J. R. Swann, E. J. Want, F. M. Geier, K. Spagou, I. D. Wilson, J. E. Sidaway, J. K. Nicholson, E. Holmes, Systemic gut microbial modulation of bile acid metabolism in host tissue compartments. *Proc. Natl. Acad. Sci. U.S.A.* **108**(Suppl. 1), 4523–4530 (2011). Medline doi:10.1073/pnas.1006734107

42. Y. Zhang, X. Ge, L. A. Heemstra, W. D. Chen, J. Xu, J. L. Smith, H. Ma, N. Kasim, P. A. Edwards, C. M. Novak, Loss of FXR protects against diet-induced obesity and accelerates liver carcinogenesis in ob/ob mice. *Mol. Endocrinol.* **26**, 272–280 (2012). Medline doi:10.1210/me.2011-1157

43. T. Inagaki, M. Choi, A. Moschetta, L. Peng, C. L. Cummins, J. G. McDonald, G. Luo, S. A. Jones, B. Goodwin, J. A. Richardson, R. D. Gerard, J. J. Repa, D. J. Mangelsdorf, S. A. Kliewer, Fibroblast growth factor 15 functions as an enterohepatic signal to regulate bile acid homeostasis. *Cell Metab.* **2**, 217–225 (2005). Medline doi:10.1016/j.cmet.2005.09.001

44. T. Li, E. Owsley, M. Matozel, P. Hsu, C. M. Novak, J. Y. Chiang, Transgenic expression of cholesterol 7alpha-hydroxylase in the liver prevents high-fat diet-induced obesity and insulin resistance in mice. *Hepatology* **52**, 678–690 (2010). Medline doi:10.1002/hep.23721

45. Y. Handelsman, Role of bile acid sequestrants in the treatment of type 2 diabetes. *Diabetes Care* **34**(Suppl. 2), S244–S250 (2011). Medline doi:10.2337/dc11-s237

46. T. R. Koves, P. Li, J. An, T. Akimoto, D. Slentz, O. Ilkayeva, G. L. Dohm, Z. Yan, C. B. Newgard, D. M. Muoio, Peroxisome proliferator-activated receptor-gamma co-activator 1alpha-mediated metabolic remodeling of skeletal myocytes mimics exercise training and reverses lipid-induced mitochondrial inefficiency. *J. Biol. Chem.* **280**, 33588–33598 (2005). Medline doi:10.1074/jbc.M507621200

47. T. R. Koves, J. R. Ussher, R. C. Noland, D. Slentz, M. Mosedale, O. Ilkayeva, J. Bain, R. Stevens, J. R. Dyck, C. B. Newgard, G. D. Lopaschuk, D. M. Muoio, Mitochondrial overload and incomplete fatty acid oxidation contribute to skeletal muscle insulin resistance. *Cell Metab.* **7**, 45–56 (2008). Medline doi:10.1016/j.cmet.2007.10.013

48. D. M. Muoio, R. C. Noland, J. P. Kovalik, S. E. Seiler, M. N. Davies, K. L. DeBalsi, O. R. Ilkayeva, R. D. Stevens, I. Kheterpal, J. Zhang, J. D. Covington, S. Bajpeyi, E. Ravussin, W. Kraus, T. R. Koves, R. L. Mynatt, Muscle-specific deletion of carnitine acetyltransferase compromises glucose tolerance and metabolic flexibility. *Cell Metab.* **15**, 764–777 (2012). Medline doi:10.1016/j.cmet.2012.04.005

49. J. S. Bakken, T. Borody, L. J. Brandt, J. V. Brill, D. C. Demarco, M. A. Franzos, C. Kelly, A. Khoruts, T. Louie, L. P. Martinelli, T. A. Moore, G. Russell, C. Surawicz; Fecal Microbiota Transplantation Workgroup, Treating Clostridium difficile infection with fecal microbiota transplantation. *Clin. Gastroenterol. Hepatol.* **9**, 1044–1049 (2011). Medline doi:10.1016/j.cgh.2011.08.014

50. P. J. Turnbaugh, V. K. Ridaura, J. J. Faith, F. E. Rey, R. Knight, J. I. Gordon, The effect of diet on the human gut microbiome: A metagenomic analysis in humanized gnotobiotic mice. *Sci. Transl. Med.* **1**, ra14 (2009).doi:10.1126/scitranslmed.3000322

51. P. P. Ahern, C. Schiering, S. Buonocore, M. J. McGeachy, D. J. Cua, K. J. Maloy, F. Powrie, Interleukin-23 drives intestinal inflammation through direct activity on T cells. *Immunity* **33**, 279–288 (2010). Medline doi:10.1016/j.immuni.2010.08.010

52. E. Esplugues, S. Huber, N. Gagliani, A. E. Hauser, T. Town, Y. Y. Wan, W. O'Connor Jr., A. Rongvaux, N. Van Rooijen, A. M. Haberman, Y. Iwakura, V. K. Kuchroo, J. K. Kolls, J. A. Bluestone, K. C. Herold, R. A. Flavell, Control of

TH17 cells occurs in the small intestine. *Nature* **475**, 514–518 (2011). Medline doi:10.1038/nature10228

53. R. C. Edgar, Search and clustering orders of magnitude faster than BLAST. *Bioinformatics* **26**, 2460–2461 (2010). Medline doi:10.1093/bioinformatics/btq461

54. J. G. Caporaso, K. Bittinger, F. D. Bushman, T. Z. DeSantis, G. L. Andersen, R. Knight, PyNAST: A flexible tool for aligning sequences to a template alignment. *Bioinformatics* **26**, 266–267 (2010). Medline doi:10.1093/bioinformatics/btp636

55. T. Z. DeSantis, P. Hugenholtz, N. Larsen, M. Rojas, E. L. Brodie, K. Keller, T. Huber, D. Dalevi, P. Hu, G. L. Andersen, Greengenes, a chimera-checked 16S rRNA gene database and workbench compatible with ARB. *Appl. Environ. Microbiol.* **72**, 5069–5072 (2006). Medline doi:10.1128/AEM.03006-05

56. J. R. Cole, B. Chai, R. J. Farris, Q. Wang, A. S. Kulam-Syed-Mohideen, D. M. McGarrell, A. M. Bandela, E. Cardenas, G. M. Garrity, J. M. Tiedje, The ribosomal database project (RDP-II): Introducing myRDP space and quality controlled public data. *Nucleic Acids Res.* **35**(Database), D169–D172 (2007). doi:10.1093/nar/gkl889 Medline

57. J. G. Caporaso, J. Kuczynski, J. Stombaugh, K. Bittinger, F. D. Bushman, E. K. Costello, N. Fierer, A. G. Peña, J. K. Goodrich, J. I. Gordon, G. A. Huttley, S. T. Kelley, D. Knights, J. E. Koenig, R. E. Ley, C. A. Lozupone, D. McDonald, B. D. Muegge, M. Pirrung, J. Reeder, J. R. Sevinsky, P. J. Turnbaugh, W. A. Walters, J. Widmann, T. Yatsunenko, J. Zaneveld, R. Knight, QIIME allows analysis of high-throughput community sequencing data. *Nat. Methods* **7**, 335–336 (2010). Medline doi:10.1038/nmeth.f.303

58. J. Kuczynski, E. K. Costello, D. R. Nemergut, J. Zaneveld, C. L. Lauber, D. Knights, O. Koren, N. Fierer, S. T. Kelley, R. E. Ley, J. I. Gordon, R. Knight, Direct sequencing of the human microbiome readily reveals community differences. *Genome Biol.* **11**, 210 (2010). Medline doi:10.1186/gb-2010-11-5-210

59. J. G. B. Oksanen, F.; Kndt, R.; Legendre, P.; Minchin, P. R.; O'Hara,R. B.; Simpson, G. L.; Solymos, P.; Stevens, M.H.H. and Wagner, H. (http://CRAN.R-project.org/package=vegan, 2011), vol. R package version 2.0-2.

60. J. J. Faith, N. P. McNulty, F. E. Rey, J. I. Gordon, Predicting a human gut microbiota's response to diet in gnotobiotic mice. *Science* **333**, 101–104 (2011). doi:10.1126/science.1206025

61. N. P. McNulty, T. Yatsunenko, A. Hsiao, J. J. Faith, B. D. Muegge, A. L. Goodman, B. Henrissat, R. Oozeer, S. Cools-Portier, G. Gobert, C. Chervaux, D. Knights, C. A. Lozupone, R. Knight, A. E. Duncan, J. R. Bain, M. J. Muehlbauer, C. B. Newgard, A. C. Heath, J. I. Gordon, The impact of a consortium of fermented milk strains on the gut microbiome of gnotobiotic mice and monozygotic twins. *Sci. Transl. Med.* **3**, ra106 (2011).doi:10.1126/scitranslmed.3002701

62. F. E. Rey, J. J. Faith, J. Bain, M. J. Muehlbauer, R. D. Stevens, C. B. Newgard, J. I. Gordon, Dissecting the in vivo metabolic potential of two human gut acetogens. *J. Biol. Chem.* **285**, 22082–22090 (2010). Medline doi:10.1074/jbc.M110.117713

63. B. Langmead, S. L. Salzberg, Fast gapped-read alignment with Bowtie 2. *Nat. Methods* **9**, 357–359 (2012). Medline doi:10.1038/nmeth.1923

64. F. Benhamed, P. D. Denechaud, M. Lemoine, C. Robichon, M. Moldes, J. Bertrand-Michel, V. Ratziu, L. Serfaty, C. Housset, J. Capeau, J. Girard, H. Guillou, C. Postic, The lipogenic transcription factor ChREBP dissociates hepatic steatosis from insulin resistance in mice and humans. *J. Clin. Invest.* **122**, 2176–2194 (2012). Medline doi:10.1172/JCI41636

65. A. L. Goodman, G. Kallstrom, J. J. Faith, A. Reyes, A. Moore, G. Dantas, J. I. Gordon, Extensive personal human gut microbiota culture collections characterized and manipulated in gnotobiotic mice. *Proc. Natl. Acad. Sci. U.S.A.* **108**, 6252–6257 (2011). Medline doi:10.1073/pnas.1102938108

66. A. L. Delcher, K. A. Bratke, E. C. Powers, S. L. Salzberg, Identifying bacterial genes and endosymbiont DNA with Glimmer. *Bioinformatics* **23**, 673–679 (2007). Medline doi:10.1093/bioinformatics/btm009

67. T. M. Lowe, S. R. Eddy, tRNAscan-SE: A program for improved detection of transfer RNA genes in genomic sequence. *Nucleic Acids Res.* **25**, 955–964 (1997). Medline

68. K. Lagesen, P. Hallin, E. A. Rødland, H. H. Staerfeldt, T. Rognes, D. W. Ussery, RNAmmer: Consistent and rapid annotation of ribosomal RNA genes. *Nucleic Acids Res.* **35**, 3100–3108 (2007). Medline doi:10.1093/nar/gkm160

69. B. L. Cantarel, P. M. Coutinho, C. Rancurel, T. Bernard, V. Lombard, B. Henrissat, The Carbohydrate-Active EnZymes database (CAZy): An expert resource for Glycogenomics. *Nucleic Acids Res.* **37**(Database), D233–D238 (2009). doi:10.1093/nar/gkn663 Medline

70. P. Boström, J. Wu, M. P. Jedrychowski, A. Korde, L. Ye, J. C. Lo, K. A. Rasbach, E. A. Boström, J. H. Choi, J. Z. Long, S. Kajimura, M. C. Zingaretti, B. F. Vind, H. Tu, S. Cinti, K. Højlund, S. P. Gygi, B. M. Spiegelman, A PGC1-α-dependent myokine that drives brown-fat-like development of white fat and thermogenesis. *Nature* **481**, 463–468 (2012). Medline doi:10.1038/nature10777

71. P. Seale, B. Bjork, W. Yang, S. Kajimura, S. Chin, S. Kuang, A. Scimè, S. Devarakonda, H. M. Conroe, H. Erdjument-Bromage, P. Tempst, M. A. Rudnicki, D. R. Beier, B. M. Spiegelman, PRDM16 controls a brown fat/skeletal muscle switch. *Nature* **454**, 961–967 (2008). Medline doi:10.1038/nature07182

72. C. Lozupone, R. Knight, UniFrac: A new phylogenetic method for comparing microbial communities. *Appl. Environ. Microbiol.* **71**, 8228–8235 (2005). Medline doi:10.1128/AEM.71.12.8228-8235.2005

73. C. A. Lozupone, M. Hamady, B. L. Cantarel, P. M. Coutinho, B. Henrissat, J. I. Gordon, R. Knight, The convergence of carbohydrate active gene repertoires in

human gut microbes. *Proc. Natl. Acad. Sci. U.S.A.* **105**, 15076–15081 (2008). Medline doi:10.1073/pnas.0807339105

74. D. Knights, E. K. Costello, R. Knight, Supervised classification of human microbiota. *FEMS Microbiol. Rev.* **35**, 343–359 (2011). Medline doi:10.1111/j.1574-6976.2010.00251.x

75. M. C. Horner-Devine, B. J. Bohannan, Phylogenetic clustering and overdispersion in bacterial communities. *Ecology* **87**(suppl.), S100–S108 (2006). Medline doi:10.1890/0012-9658(2006)87[100:PCAOIB]2.0.CO;2

76. J. P. Furet, L. C. Kong, J. Tap, C. Poitou, A. Basdevant, J. L. Bouillot, D. Mariat, G. Corthier, J. Doré, C. Henegar, S. Rizkalla, K. Clément, Differential adaptation of human gut microbiota to bariatric surgery-induced weight loss: Links with metabolic and low-grade inflammation markers. *Diabetes* **59**, 3049–3057 (2010). Medline doi:10.2337/db10-0253